arXiv:1107.2119v2 [astro-ph.CO] 23 Sep 2011

Non-thermal Processes in Black-Hole-Jet Magnetospheres

Frank M. Rieger

Max-Planck-Institut für Kernphysik, 69117 Heidelberg, Germany,
and European Associated Laboratory for Gamma-Ray Astronomy, jointly supported by CNRS
and MPG
frank.rieger@mpi-hd.mpg.de

The environs of supermassive black holes are among the universe's most extreme phenomena. Understanding the physical processes occurring in the vicinity of black holes may provide the key to answer a number of fundamental astrophysical questions including the detectability of strong gravity effects, the formation and propagation of relativistic jets, the origin of the highest energy gamma-rays and cosmic-rays, and the nature and evolution of the central engine in Active Galactic Nuclei (AGN). As a step towards this direction, this paper reviews some of the progress achieved in the field based on observations in the very high energy domain. It particularly focuses on non-thermal particle acceleration and emission processes that may occur in the rotating magnetospheres originating from accreting, supermassive black hole systems. Topics covered include direct electric field acceleration in the black hole's magnetosphere, ultra-high energy cosmic ray production, Blandford-Znajek mechanism, centrifugal acceleration and magnetic reconnection, along with the relevant efficiency constraints imposed by interactions with matter, radiation and fields. By way of application, a detailed discussion of well-known sources (Sgr A*; Cen A; M87; NGC1399) is presented.

Keywords: Black Hole, Magnetosphere, Particle Acceleration, Radiation Mechanism, Gamma-Rays, Cosmic Rays.

1. INTRODUCTION

This review focuses on non-thermal particle acceleration and very high energy (VHE) emission processes that may occur in the vicinity of magnetized supermassive black holes. As such, active galaxies and, to some extent, extinct or dormant quasars are placed in the center of its attention. Although rotating, supermassive black holes have often been considered as putative sources for the energization of ultra-high energy (UHE) cosmic rays, non-thermal magnetospheric models have recently gained an additional impetus with the detection of very high energy gamma-rays from the (non-blazar) radio galaxy M87, located $\sim$ 16 Mpc away in the Virgo cluster of galaxies.[1,2,3] While former observations of rapid VHE flux variations (on timescales of $\sim [1-2]$ days) already indicated a small size of the γ-ray emitting region, the location of this region remained ambiguous based on the VHE results alone. Additional high-resolution ($\sim$ 50 Schwarzschild radii) radio VLBA imaging has now

shown that the gamma-ray flaring activity is accompanied by an increase in the radio flux close to core (see Fig. 1), indicating that the required energetic charged particles may in fact be accelerated in the very vicinity of the central black hole.[4] At present, further evidence is needed to strengthen this inference. Nevertheless, magnetospheric models where the relevant non-thermal processes are considered to occur at the base of a rotating black-hole-jet magnetosphere (e.g., refs.[5,6,7]), have emerged as attractive candidates. If verified by further observations, VHE gamma-ray observations could provide a fundamental diagnostic of the most violent region in Active Galactic Nuclei (AGN).

 This review is structured as follows: Sect. 2 gives a phenomenologically-orientated introduction into the close environment of supermassive black holes. In Sect. 3, particle acceleration scenarios that draw on rotating, large-scale poloidal magnetic fields (i.e., the magnetosphere) are presented. Sect. 4 discusses possible interactions of accelerated particles with ambient matter, radiation and fields, that are expected to limit achievable particle energies. Applications to concrete sources as potential VHE gamma-ray and UHE cosmic ray emitters are discussed in Sect. 5.

2. SUPERMASSIVE BLACK HOLES AND MAGNETIC FIELDS

2.1. *Evidence and Mass Range*

Most, if not all galaxies, are nowadays believed to harbor a supermassive black hole (BH) with 10^6 to $10^{9.5} M_\odot$ at their center[8,9] (for reviews see also refs.[10,11]). Initially hypothesized in order to account for the huge power output seen from extragalactic radio sources such as quasars,[12] the presence of supermassive black holes has now directly been probed by a variety of means, e.g., through the velocity dispersion of stars, water maser line emission or the kinematics of nearby ionized gas. The most prominent example is probably the center of our own galaxy where near-infrared imaging revealed proper motion of stars which increases with a Kepler law down to separations of less than five light days from the compact radio source Sgr A*, thus providing strong evidence for the presence of a black hole of mass $\simeq 3 \times 10^6 M_\odot$.[13,14] Several important correlations for the black hole masses in galaxies have been established within recent years, including (i) a relation between the black hole mass and the luminosity/mass of its host galaxy bulge, e.g., $M_{\rm BH} \simeq 2 \times 10^{-3} M_{\rm bulge}$, and (ii) a relation between the black hole mass and the host galaxy stellar velocity dispersion σ, $\log(M_{\rm BH}/M_\odot) = (8.21 \pm 0.06) + (3.83 \pm 0.21) \log(\sigma/200 \text{ km/s})$ (with intrinsic scatter of 0.22 ± 0.06 dex).[15] For the nearby (z=0.034) gamma-ray blazar Mkn 501 (HBL source), for example, $\sigma = 291 \pm 13$ km/s has been found,[16] suggesting a central black hole mass of $\gtrsim 3 \times 10^8 M_\odot$. Similarly, observations of the giant elliptical radio galaxy NGC 1399 in the centre of the Fornax cluster ($d \sim 20$ Mpc) suggest $\sigma \simeq 320$ km/s,[17] indicating the presence of a black hole with mass exceeding $\sim 5 \times 10^8 M_\odot$ (see also ref.[18]).
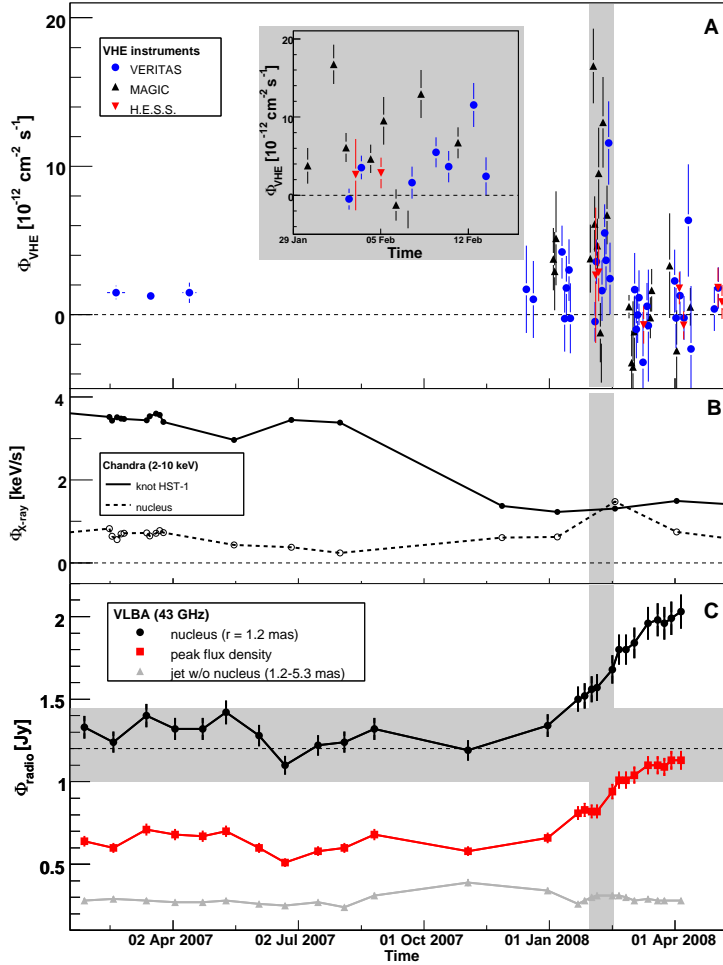
Fig. 1.   Combined VHE gamma-ray, X-ray and radio light curves for the radio galaxy M87 in 2007–2008. A VHE gamma-ray flare (Fig. A) is followed by an increase of the radio flux (Fig. C) close to the black hole. Knot HST-1, located in the jet ~ 100 pc away, is in a low X-ray state (Fig. B) and therefore unlikely to be the source of the observed VHE gamma-rays. Details are as follows: (A) VHE -ray flux data ($E > 0.35$ TeV, nightly average) including H.E.S.S., MAGIC, and VERITAS. The inlay shows a zoomed version of the rapid flaring activity (with timescales as low as $\sim [1 - 2]$ days) in February 2008. (B) X-ray (Chandra) flux for the nucleus and the knot HST-1. (C) Radio (43 GHz VLBA) flux data. The shaded horizontal area indicates the range of radio fluxes from the nucleus before the 2008 flare. The radio flux of the outer jet regions does not change substantially; most of the observed increase results from the region around the nucleus. Figure adapted from Acciari et al.[4]

2.2. *Rotating Black Holes*

Supermassive black holes residing in the centers of galaxies may be driven into rotation by prolonged accretion of angular momentum or as a result of merger
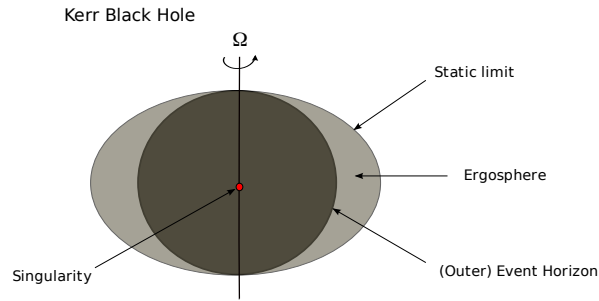
4   *F.M. Rieger*

Fig. 2.   Schematic drawing of the structure of a rotating Kerr black hole.

events.

2.2.1. *Characteristic properties*

The angular momentum J for a (rotating) Kerr black hole of mass M is usually expressed in terms of the dimensionless spin parameter $a \leq 1$, $J = a\, J_{\max}$, where the maximum value $J_{\max}$ is given by

$$J_{\max} = \frac{GM^2}{c}\,. \tag{1}$$

so that an extreme (maximally spinning) Kerr black hole is characterized by a spin parameter

$$a = \frac{J}{GM^2/c} = \frac{J}{J_{\max}} = 1\,. \tag{2}$$

For a non-rotating (Schwarzschild) black hole we have $J = a = 0$, and the event horizon scale r_H coincides with the Schwarzschild radius

$$r_{\mathrm{s}} = \frac{2GM}{c^2} \simeq 3 \times 10^{13} \left(\frac{M}{10^8 M_\odot} \right)\ \mathrm{cm}\,. \tag{3}$$

For a rotating Kerr black hole the (spherical) event horizon surface is located at

$$r_H = \frac{r_s}{2} \left(1 + \sqrt{1 - a^2} \right)\,, \tag{4}$$

with $0 \leq a \leq 1$, and where $r_g = r_{\mathrm{s}}/2$ is often called the gravitational radius. Hence, for a Schwarzschild black hole $r_H = r_{\mathrm{s}}$ and for an extreme Kerr black hole $r_H = r_g$.

The static limit r_E is situated at

$$r_E = \frac{r_s}{2}\left(1 + \sqrt{1 - a^2 \cos^2\theta}\right) \tag{5}$$

where θ is the angle to the polar axis. The region between $r_H < r < r_E$ is called the ergosphere. Within the ergosphere (which is ellipsoidal in shape), space-time is dragged along in the direction of the hole's rotation (frame dragging), so that no static observer can exist and a particle has to co-rotate with the hole. The angular velocity Ω_H of a black hole is defined as the angular velocity of the dragging of inertial frames at the horizon and given as

$$\Omega_H = a\left(\frac{c}{2r_H}\right), \tag{6}$$

so that for an extreme Kerr black hole $\Omega_H = c/2r_g$.

A rotating black hole possesses an additional source of energy, which for low spin parameters a is given by $E_{\rm rot} = (1/2)I_H\Omega_H^2 = (1/8)a^2 Mc^2$ where the black hole's moment of inertia $I_H = Mr_H^2$ has been employed. For general spins, the maximum rotational energy $E_{\rm rot}$ of a rotating black hole can be expressed as the difference between the total mass-energy Mc^2 and its irreducible mass $M_{\rm irr}c^2$, see refs.[19,20],

$$E_{\rm rot} = (M - M_{\rm irr})c^2 = Mc^2\left(1 - \sqrt{0.5\left(1 + \sqrt{1 - a^2}\right)}\right) \leq 0.29 Mc^2\,. \tag{7}$$

Thus, if supermassive black holes would indeed be rapidly rotating and if they would be able to dissipate all of their rotational energy over a characteristic life time $t_{\rm Edd} = 4.5 \times 10^7$ yr (see Eq. [11]), this could yield a considerable luminosity output

$$L_{\rm rot} = \frac{E_{\rm rot}}{t_{\rm Edd}} \leq 3.6 \times 10^{46}\left(\frac{M}{10^8 M_\odot}\right)\ {\rm erg/s}\,, \tag{8}$$

comparable in magnitude to the Eddington luminosity (see Eq. [9]). The maximum output is, however, very sensitive to the spin parameter a. For moderate spins, e.g., $a = 0.5$, it is already about an order of magnitude smaller ($E_{\rm rot} = 0.034 Mc^2$), see Fig. (3) for illustration.

Note that the most general, stationary black hole metric is the Kerr-Newman metric, where the black hole is described by its mass M, electric charge Q and spin angular momentum J. Special cases are the Kerr ($Q = 0, J \neq 0$), the Reissner-Nordström ($J = 0, Q \neq 0$) and the Schwarzschild ($J = Q = 0$) black hole. Charged black holes are commonly thought not to be of astrophysical importance (but see also, e.g., refs.[21,22]), as the surrounding plasma is usually expected to rapidly neutralize any charge imbalance (e.g., refs.[23,24]).[a]

---

[a]The metric function implies the constraint $(J/M)^2 + (GQ^2/c^2) \leq (GM/c)^2$, so that the maximum, theoretically possible charge would be $Q_m = G^{1/2}M$. However, real astrophysical black holes are expected to possess only negligible charge (i.e., $Q \lesssim GMm_p/e \sim 10^{-18}Q_m$) as otherwise electric forces would dominate over gravitational ones, enabling charge separation and attracting opposite charge to neutralize the imbalance. This implies that the magnetic field produced by a charged black hole is limited to $B \lesssim m_p c^2/(er_g) \sim 2 \times 10^{-7}(10^8 M_\odot/M)$ G.
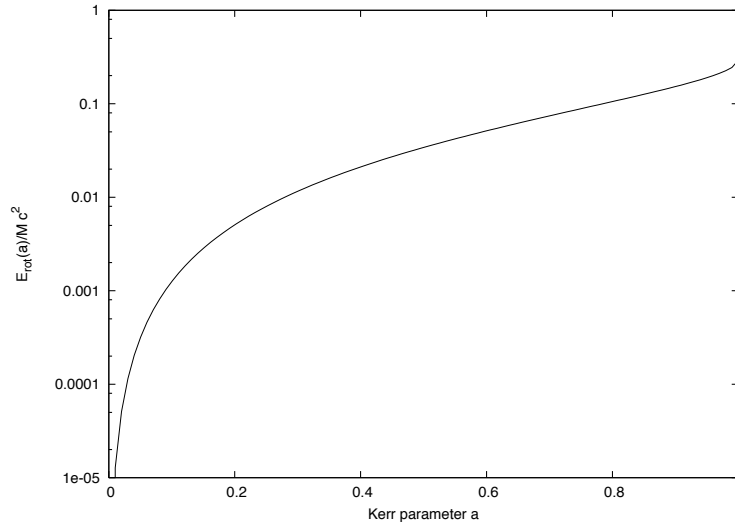
Fig. 3.   Maximum extractable energy of rotating black hole as a function of the dimensionless spin parameter a.

2.2.2. *On the Distribution of Black Hole Spins*

Despite their obvious significance, the spins of astrophysical (supermassive) black holes have been proven difficult to pin down unambiguously. This may appear somewhat unfortunate, as it e.g. directly affects inferences about the maximum rotational energy that could possibly be extracted by some electrodynamic processes (cf. Eq. [7]). Naively, one expects that supermassive black holes can be spun-up by prolonged accretion of angular momentum or by the merger of black holes with similar masses (having high orbital angular momentum). On the other hand, if a rotating black hole would be able to emit a strong (persistent) spin-powered jet of, e.g., $L_j \sim 10^{46}(M/10^8 M_\odot)$ erg/s, the hole's rotation could spin down on an e-folding timescale $E_{\rm rot}/L_j \sim 10^8$ yr comparable to the typical AGN lifetime. Then again, prolonged accretion or further merger events could help to sustain high black hole spins. Prolonged accretion is expected to lead to high spins $(a \sim 1)$,[25] whereas major mergers tend to produce average spins of $\langle a \rangle \sim 0.7$.[26] Provided accretion is not inherently random and episodic, cosmological N-body simulations suggest that the final black hole spin depends almost exclusively on the accretion history and very little on the merger history.[27] Accordingly, more massive black holes (i.e., those hosted by elliptical galaxies) should be characterized by higher spin parameters (average $\langle a \rangle \geq 0.8$ at $z = 0$) compared to those residing in, e.g. spirals. However, the underlying assumption of a spin evolution via prolonged accretion has been questioned recently.[28] In the standard picture, Lense-Thirring precession is assumed to always ensure co-alignment of the disk with the black hole spin, and thus to lead to spin-up via prograde accretion.[29] However, this needs not necessarily to be the

case if the disk is sufficiently small. Instead, accretion may then be random and episodic in character, so that the spins are expected to readily adjust to average values $\langle a \rangle \sim 0.1 - 0.3$. Such a spin-down scenario seems in fact supported by recent studies of the radiative efficiency from accretion onto supermassive black holes:[b] (i) Existing quasar survey data suggest a significant decrease of the radiative efficiency from high ($\eta \sim 0.2 - 0.3$ at $z \simeq 2$) to low redshift ($\eta \sim 0.03$ at $z = 0$). While the spin evolution at $z \sim 2$ may be driven by major merger events, the decrease of the radiative efficiency towards low z seems to support an interpretation according to which black holes are fed by accretion events that tend to spin down the black hole over time ($a \sim 0$ at $z = 0$).[31] (ii) Similarly, a rather low mean efficiency $\langle \eta \rangle \sim 0.07$ has been inferred based on the cumulative energy density emitted by AGNs over the age of the Universe. The results indicate $\langle a \rangle \simeq (0.2 - 0.6)$ and suggest that supermassive black holes are on average not rapidly spinning during accretion.[32] Note that if Maxwell stresses do (contrary to what is usually assumed) not vanish at r_{ms}, as in fact seen in recent MHD disk simulations,[33] this could lead to an excess dissipation, lowering the above inferred spins even more (possible differences seem to be small, though, at least in the case of a thin disk[34]).

Yet, while on average rather moderate values of a seem to be preferred, a subpopulation of AGNs with high spins may well exist. In fact, X-ray observations of relativistically broad iron Kα lines from the black hole's vicinity, e.g., in the prominent Seyfert 1 galaxy MCG-6-30-15, for which $a > 0.9$ has been inferred, indicate that at least some radio-quiet (!) AGN may harbor rapidly spinning black holes (for review, see refs.[35,36]).[c] If indeed the case, then this implies that a high black hole spin is not a sufficient condition for radio-loudness as initially suggested by Wilson & Colbert[39]. On the other hand, evidence for rather low black hole spins in the galactic microquasar sources XTE J1550-564 ($a \simeq 0.1$) and A0620-00 ($a \simeq 0.3$) also challenge the common perception that black hole spins and relativistic jets are necessarily connected.[40] Fender et al.[41] have recently concluded that at least for galactic black hole X-ray binaries (which are often believed to be scaled-down versions of AGNs), there is no evidence for either the jet power or the jet speed being related to the spin of the black hole. If this is indeed the case, it may point to the fact that the jets rather emerge as centrifugally-driven (Blandford-Payne) outflows from the accretion disk.

With this caveat in mind, estimates for the jet kinetic power (e.g., from intraclus-

---

[b]The radiative efficiency η is usually defined as $\eta = 1 - e_{\mathrm{ms}}/c^2$, where $e_{\mathrm{ms}} = c^2(1 - r_s/3r_{\mathrm{ms}})^{1/2}$ is the binding or specific energy of a test particle rotating in the innermost stable circular orbit at r_{ms}, and becomes $\eta = 0.057$ for a Schwarzschild and $\eta = 0.42$ for an extreme Kerr black hole ($a = 1$). Note that while accretion by itself would spin up the black hole rather quickly to its maximum value $a = 1$, photon capture will prevent complete spin-up and limit the maximum spin to $a = 0.998$. While this is still very close to $a = 1$, it has a significant effect on the maximum possible radiative efficiency, reducing it to $\eta = 0.3$.[30]
[c]Note however, that recent modelling of the broad iron lines in the Seyfert-1 AGNs Fairall 9 and Swift J2127.4+5654 seems to favor more moderate spin values $a \sim 0.6$, making MCG-6-30-15 appear somewhat exceptional.[37,38]

ter X-ray cavities inflated by the radio jets) and for the central black hole mass have been employed to constrain the spin parameters for selected samples of radio galaxies. Some of these studies conclude that the radio-loud dichotomy of FR I and FR II radio galaxies can be reproduced by a transition in accretion mode from a standard disk to an ADAF, with the black holes for both classes rapidly rotating $(a \gtrsim 0.9)$.[42,43] Others instead find that the FR I type and FR II sources they studied are consistent with spin values of $a \simeq (0.01 - 0.4)$ and $a \simeq (0.2 - 1)$, respectively, and report evidence for a decrease of the black hole spin in FR II with decreasing redshift.[44] At present, further studies are certainly needed to clarify this issue.

2.3. *Accretion onto Black Holes*

2.3.1. *Spherical accretion and Eddington constraints*

The luminosity of an accretion-powered object of mass M cannot grow indefinitely. In the case of steady spherical accretion, the maximum luminosity is limited to the Eddington value L_{Edd} given by the balance between (outward-directed) radiation-pressure and (inward-directed) gravitational force,

$$L_{\text{Edd}} = \frac{4\pi c G M m_p}{\sigma_T} = 1.25 \times 10^{46} \left(\frac{M}{10^8 M_\odot}\right) \text{erg/s} . \qquad (9)$$

The critical accretion rate required to sustain the Eddington luminosity, assuming a typical $\eta = 0.1$ efficiency of conversion of mass to radiant energy, is then defined as

$$\dot{M}_{\text{Edd}} = \frac{L_{\text{Edd}}}{\eta c^2} \simeq 1.4 \times 10^{26} \left(\frac{M}{10^8 M_\odot}\right) \text{g/s} \simeq 2.2 \left(\frac{M}{10^8 M_\odot}\right) M_\odot \, \text{yr}^{-1} . \qquad (10)$$

The Eddington timescale (sometimes called the Salpeter timescale) is the e-folding growth time for the mass of a black hole accreting at the Eddington rate

$$t_{\text{Edd}} = \frac{M}{\dot{M}_{\text{Edd}}} = 4.5 \times 10^7 \text{yr} . \qquad (11)$$

The fiducial Eddington magnetic field upper limit B_{Edd} has an energy density equal to the radiative energy density at r_g of a body emitting at L_{Edd}, i.e., $B = (2L_{\text{Edd}}/r_g^2 c)^{1/2}$,

$$B_{\text{Edd}} \simeq 6.1 \times 10^4 \left(\frac{10^8 M_\odot}{M}\right)^{1/2} \text{G} . \qquad (12)$$

2.3.2. *Standard, steady state accretion flows*

In general, the structure of an accretion flow is determined by the balance between gravitational heating and cooling. Its concrete structure therefore depends on what kind of heating and cooling processes are assumed to be dominating. In the classical approach of Shakura & Sunyaev[45], commonly referred to as the *standard accretion disk model*, the disk is flat (geometrically thin: $H \ll r$; H the half thickness of the

disk, r the radial distance) and opaque (optically thick in vertical direction). Viscous (frictional) stresses[d] are assumed to convert gravitational potential energy into heat that is released locally in the form of a thermal black body spectrum $B_\nu(T_{\text{eff}}[r])$ (i.e., possible modifications by advection or a jet are neglected) with energy flux per unit surface area of $F(r) = \pi \int B_\nu(T_{\text{eff}}[r])d\nu = \sigma T_{\text{eff}}(r)^4$ and characteristic effective temperature

$$T_{\text{eff}}(r) = \left[\frac{3GM\dot{M}}{8\pi\sigma r^3} \left(1 - \sqrt{\frac{r_{\text{in}}}{r}} \right) \right]^{1/4}$$

$$= 6.3 \times 10^5 \left(\frac{\dot{M}}{\dot{M}_{\text{Edd}}} \right)^{1/4} \left(\frac{10^8 M_\odot}{M} \right)^{1/4} \left(\frac{r_s}{r} \right)^{3/4} \left(1 - \sqrt{\frac{r_{\text{in}}}{r}} \right)^{1/4} \text{K} \,. \quad (13)$$

Far from the inner edge, $r \gg r_{\text{in}}$, the temperature approximately obeys $T_{\text{eff}}(r) \propto r^{-3/4}$. As gravity is stronger on smaller scales, the disk surface is hotter in the inner region. The radially integrated disk luminosity is

$$L_d = 2 \int_{r_{\text{in}}}^{r_{\text{out}}} 2\pi r F(r) \, dr \simeq \frac{GM\dot{M}}{2r_{\text{in}}} = \frac{1}{4} \left(\frac{r_s}{r_{\text{in}}} \right) \dot{M}c^2 \,. \quad (14)$$

Half of the total gravitational energy release $GM\dot{M}/r_{\text{in}}$ is thus radiated away, the remaining half being accounted for by the kinetic energy of the orbiting material. The emerging disk spectrum $F_\nu \propto \int B_\nu(T_{\text{eff}}[r])r dr$ can be obtained by integrating B_ν over the surface of the disk. The resultant spectrum is shown in Fig. 4: It initially rises with ν^2, then flattens (provided the disk is large enough) in the intermediate region to $\nu^{1/3}$, before it decays exponentially towards the highest frequencies. For characteristic AGN parameters, the emission from the inner part is maximized at a frequency

$$\nu_{\text{max}} = \frac{2.82kT_{\text{eff}}}{h} \simeq 5.9 \times 10^{15} \left(\frac{T_{\text{eff}}}{10^5 \text{ K}} \right) \text{Hz} \,, \quad (15)$$

suggesting that this type of accretion flow could lead to a 'big blue bump' feature, i.e. a significant optical/UV disk contribution to the observed SED.
As a consequence of the viscous interactions between adjacent layers in the disk, angular momentum is transferred outwards, while mass falls (accretes) inwards.

2.3.3. *Inner edge of the accretion disk*

In the classical picture, the radius of the inner edge r_{in} of the standard disk extends down to the (innermost) marginally stable circular orbit $r_{\text{in}} = r_{\text{ms}}$. Inside r_{ms} space-time gets so strongly curved that stable orbits no longer exist. A particle thus unavoidably falls into the black hole. This is why the region inside r_{ms} is often

---

[d]With the rϕ-component of the shear stress tensor taken to be proportional to the total (gas and radiation) pressure p, i.e., $t_{r\phi} = \alpha p$, $\alpha \le 1$ (α-prescription).
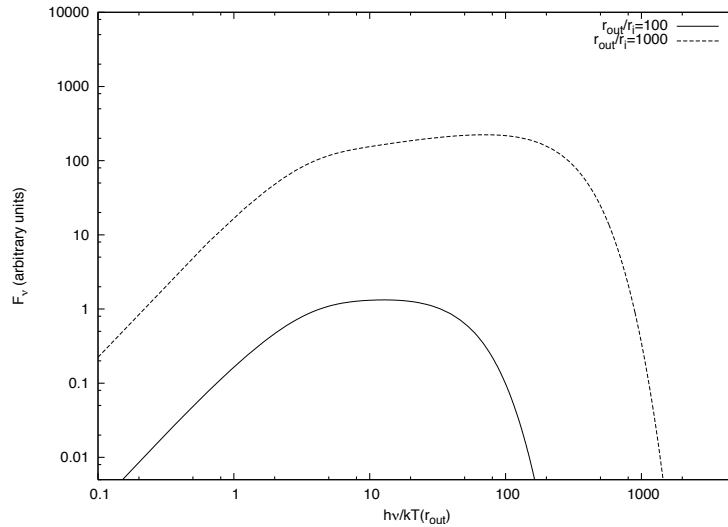
Fig. 4.   The characteristic continuum spectrum of a standard, geometrically thin, optically thick disk for two different outer radii r_{out}. The spectrum is normalized to $h\nu/kT(r_{\mathrm{out}})$. If the disk is not large enough, e.g., for $r_{\mathrm{out}}/r_{\mathrm{in}} = 100$, the $\nu^{1/3}$–power law part may not become apparent.

called the "plunging region" as gas can spiral into the black hole without further loss of angular momentum. The analytical solution for the innermost stable orbit as a function of the dimensionless spin parameter a is given by[46]

$$r_{\mathrm{ms}} = \frac{r_s}{2}\left[3 + Z_2 \mp \sqrt{(3 - Z_1)(3 + Z_1 + 2Z_2)}\right] \qquad (16)$$

where

$$Z_1 = 1 + (1 - a^2)^{1/3}\left[(1 + a)^{1/3} + (1 - a)^{1/3}\right]$$

$$Z_2 = \sqrt{3a^2 + Z_1^2}\,. \qquad (17)$$

Hence, for a Schwarzschild black hole ($a = 0$), $r_{\mathrm{ms}} = 3r_s = 6r_g$, while for the extreme Kerr case ($a = 1$), $r_{\mathrm{ms}} = r_s/2 = r_g$ (prograde orbit) or $r_{\mathrm{ms}} = 9r_s/2 = 9r_g$(retrograde orbit). As mentioned above, the disk's radiative efficiency is strongly dependent on the position of its innermost radius.

2.3.4. *Radiatively inefficient accretion flows*

In the standard approach, cooling is so efficient that all the energy released through viscosity is radiated away locally. This may not always be the case and in fact we know steady disk solutions where this assumption is violated (for a review, see Kato et al.[47]). In the case of a radiatively inefficient accretion flow (RIAF), for example, most of the energy released is stored within the flow and transported inward with accretion. While the disk thus locally undergoes advective cooling, the flow itself becomes very hot. When the density of the accretion flow falls below

a critical value, the flow becomes optically thin and the efficiency for radiative cooling (e.g., bremsstrahlung, which dominates at non-relativistic temperatures) becomes small. The classical RIAF prototype is the two-temperature, optically-thin advection-dominated accretion flow (ADAF) model (for review, see refs.[48,49]). By assumption, the released viscous energy is assumed to go primarily into ion heating, while cooling is mainly by the electrons. If the densities are sufficiently low, Coulomb coupling between protons and electron is weak and the viscous energy transfer from protons to electrons becomes very small, limiting the amount of energy that can be lost by radiation. This introduces a critical accretion rate

$$\dot{M} \sim \alpha^2 \dot{M}_{\mathrm{Edd}} \tag{18}$$

above which an ADAF cannot exist (typically, $\alpha \sim 0.2 - 0.3$). Because of the very high temperature ($T_p \sim GMm_p/3k_B r \sim 3 \times 10^{12}(r_g/r)$ K for ions, $T_e \sim 5 \times 10^9$ K for electrons) ADAFs are marginally geometrically thick with scale height $H/r \sim 1$ at every radius, independent of the accretion rate. The total radiative luminosity of an ADAF is found to be proportional to the square of the mass accretion rate, in contrast to the standard thin disk where $L \propto \dot{M}$ (eq. [14]), i.e.

$$L_{\mathrm{ADAF}} \sim \frac{2 \times 10^{-2}}{\alpha^2} \left(\frac{\dot{M}}{\dot{M}_{\mathrm{Edd}}} \right) \dot{M} c^2 \propto \dot{M}^2 \tag{19}$$

(Mahadevan 1997), and thus can be much smaller than the luminosity expected from a standard disk. The broadband spectrum emerging from an ADAF can cover the energy range from radio to hard X-ray frequencies, see Fig. 5. The radio to sub-mm regime is typically produced by synchrotron emission of relativistic thermal electrons and in its optically thin part rises with $L_\nu \propto \nu^{2/5}$.[50] The emission at the highest peak frequency ν_p comes from the innermost part of the disk[50,49]

$$\nu_p(r) \simeq 10^{12} \left(\frac{10^8 M_\odot}{M} \right)^{1/2} \left(\frac{\dot{M}}{0.01 \dot{M}_{\mathrm{Edd}}} \right)^{1/2} \left(\frac{T_e}{10^9 \mathrm{K}} \right)^2 \left(\frac{r_s}{r} \right)^{5/4} \mathrm{Hz}, \tag{20}$$

while the lower frequency synchrotron emission originates from further out. Compton upscattering of the low-energy synchrotron photons by the relativistic thermal disk electrons results in a hard power law tail extending up to energies of $h\nu \sim kT_e \sim (100 - 500)$ keV. Compton scattering becomes less important with decreasing accretion rates, and the spectrum becomes steeper (softer). For sufficiently low $\dot{M}$ distinct Compton peaks can appear. This is related to the increase in electron temperature with decreasing accretion rates. For low $\dot{M}$, the X-ray spectrum is dominated by bremsstrahlung emission (with a non-negligible contribution from large radii) due to electron-electron and electron-ion interactions, again up to a maximum energy of $\sim kT_e$, beyond which the spectrum falls off exponentially.[51]

A number of additional scenarios have been discussed in the literature that extend and complement the classical ADAF picture described above. One important modification concerns, e.g., jets and winds. Since for self-similar ADAFs the net energy
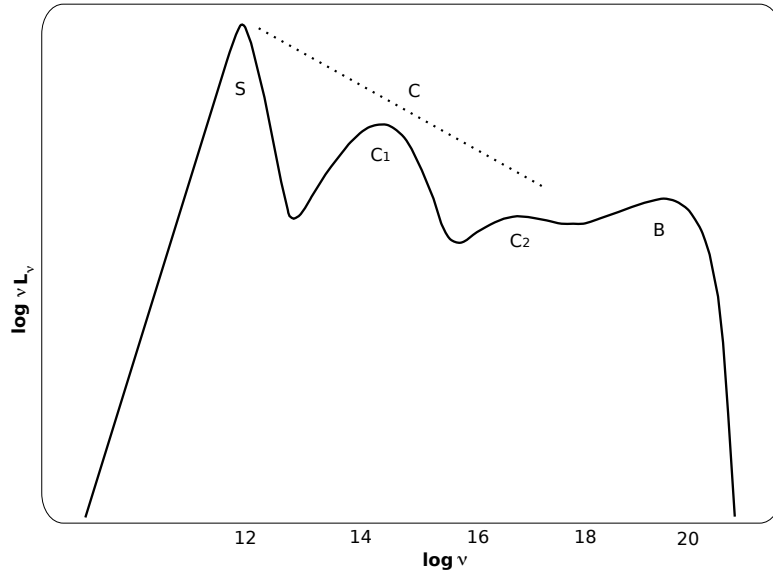
Fig. 5. Sketch of a typical ADAF spectrum around a supermassive black hole. Synchrotron emission (S) of the relativistic thermal electrons produces a peak at around 10^{12} Hz. At moderate accretion rates, Comptonization results in a power-law tail (C) extending into the X-ray domain. For low accretion rates, distinct Compton (C1=once Compton scattered, C2=twice Compton scattered) peaks appear. The X-ray/soft gamma-ray regime is usually dominated by bremsstrahlung emission (B), peaking at $h\nu \simeq kT_e$, and with luminosity scaling as $L_{\mathrm{br}} \propto \dot{m}^2$.

of the accretion flow can remain positive and unbound to the central object (positive Bernoulli number),[52] strong outflows may well form and modify the emergent spectra, cf. the ADIOS model by Blandford & Begelman[53]. While the positiveness of the Bernoulli number is a necessary (but not sufficient) condition for outflows, 2-D simulations indeed suggest that for large viscosity parameters ($\alpha \gtrsim 0.3$) strong outflows can occur.[54,55] If mass is supplied by an outer standard disk, ADIOS-like outflows may however only occur for transition radii $r_t \gtrsim 100 r_s$.[56]

2.4. *Magnetic Field Strengths*

In the standard disk case, we can derive a characteristic (maximum local equipartition) magnetic field strength close to r_g, whose energy density is comparable to that of the radiation (i.e., $B^2/8\pi = \sigma T_{\mathrm{eff}}^4/c$) which gives (cf. eq. [13])

$$B_r \simeq 4.4 \times 10^4 \left(\frac{\dot{M}}{\dot{M}_{\mathrm{Edd}}} \right)^{1/2} \left(\frac{10^8 M_\odot}{M} \right)^{1/2} \mathrm{G} \,. \tag{21}$$

For $\dot{M} = \dot{M}_{\mathrm{Edd}}$ this is of about the same strength as the Eddington equipartition magnetic field B_{Edd}, eq. (12), obtained by assuming that all of L_{Edd} emerges from r_g. In the case of an advection-dominated accretion flow (ADAF) on the other

hand, the characteristic equipartition magnetic field is given by $B_a^2/8\pi \simeq 0.5\rho c_s^2$. Here c_s denotes the isothermal sound speed, $\rho \propto \dot{M}/(r^2 v_r)$ is the density of accreted matter, $v_r \sim 0.5\alpha v_f$ is the typical radial infall speed and $v_f = (GM/r)^{1/2}$ the free fall velocity. When scaled to the AGN mass range, this becomes[48]

$$B_a \simeq 7.8 \times 10^4 \; \alpha^{-1/2} \left(\frac{\dot{M}}{\dot{M}_{\mathrm{Edd}}} \right)^{1/2} \left(\frac{10^8 M_\odot}{M} \right)^{1/2} \left(\frac{r}{r_s} \right)^{-5/4} \mathrm{G} \,. \qquad (22)$$

As an ADAF cannot exist above $\dot{M} \sim \alpha^2 \dot{M}_{\mathrm{Edd}}$, cf. eq. (18), the maximum B_a is comparable to the maximum B_r in the standard case.

Note that the poloidal field strength in the magnetosphere may be significantly smaller than these disk field values. Taking B_r to be characteristic for the poloidal magnetospheric field component, for example, may then well overestimate the possible power of a Blandford-Znajek-type process. It has in fact been argued,[57] that the large-scale poloidal field B_{pd} threading the disk should be related to the small scale field produced by dynamo processes via $B_{\mathrm{pd}} \sim (H/r)B_{\mathrm{dynamo}}$, where H/r is the typical disk scale height, which for a standard disk is much smaller than unity (cf. however also ref.[58]). In any case, as the field threading the hole is generated by currents in the disk, it seems unlikely that its strength should significantly exceed the field threading the inner disk.

2.5. *Black Hole-Jet-Magnetospheres*

Once a spinning black hole or disk becomes threatened by an ordered (large-scale poloidal) magnetic field, it can build up a rotating magnetosphere filled up with currents. The required magnetic flux could be advected from the interstellar magnetic field via the accretion process and/or be produced (amplified) through dynamo actions in the inner accretion disk.[e] While this picture may appear qualitatively evident, the detailed electromagnetic structure of the magnetosphere is a highly complex problem. Most research has been influenced by the seminal papers of Blandford & Znajek (BZ)[60] and Blandford & Payne[61]. Roughly speaking, the main difference concerns the question whether the source of rotational energy and angular momentum lies with the black hole's rotation or with the accretion disk. Methodologically, this often translates into two different approaches (for review and further references, see e.g. refs.[62,63]):

In the first, the *force-free electrodynamic* (FFE) approximation, the magnetospheric structure is assumed to be governed by Ampere's and Faraday's law and to be force-free everywhere (i.e., dominated only by magnetic and electric stresses). Accordingly, gravitational and inertial forces are neglected (massless limit of MHD)

---

[e]An alternative scenario relates to the Poynting-Robertson radiation force acting predominantly on the electrons in the accretion disk. As a consequence, electrons lag behind the protons, and a toroidal electric current develops that can become sufficiently large to produce significant poloidal magnetic fields.[59]

and the current density $\vec{j}$ perpendicular to the local magnetic field is determined from the force-free condition $\rho \vec{E}_\perp + \vec{j} \times \vec{B}/c = 0$, where ρ is the charge density.[64] This approximation quite simplifies the standard problem in that it allows to solve for the electromagnetic field structure without having to solve for the plasma dynamics. Magnetic field lines may then be thought as (quasi-rigidly) rotating with the angular velocity Ω of the horizon or the inner disk (Ferraro's law). Approaching the light surface where $|\vec{\Omega} \times \vec{r}| = c$ the field is swept backwards opposite to the sense of rotation and a toroidal twist is introduced. By assumption, plasma in the magnetosphere is streaming outward at almost the speed of light, its only role being to provide the currents required to sustain the magnetic field.

In the second approximation, the *relativistic MHD (single fluid) approach*, the force-free condition is modified to allow for inertial and pressure terms in the equation of motion. If plasma loading is not negligible, as may be the case for field lines connecting to the disk, such a modification appears unavoidable. The system is then closed by Ohm's law asserting that the current density $\vec{j}$ is proportional to the electric field $\vec{E}' = \vec{E} + \vec{v} \times \vec{B}/c$ seen in the frame where the fluid is at rest. In the high conductivity (ideal MHD) limit, $\sigma_e \to \infty$, Ohm's law implies $\vec{j}/\sigma_e = \vec{E} + \vec{v} \times \vec{B}/c \to 0$ where $\vec{v}$ is the fluid velocity. Within the Alfvén surface[f] plasma that becomes attached to the field lines behaves like a bead on a wire and is flung out by the centrifugal force given suitable field line orientations (e.g., inclinations wrt to disk launching of less than $60°$ in Newtonian approximation, and nearly $90°$ in the extreme Kerr limit.[65,66,67]). For stationary and axisymmetric configurations, the equation of motion (which in the low inertia limit just reduces to the force-free condition) projected perpendicular to the field lines gives the famous Grad-Shafranov equilibrium (ideal MHD) equation. The so-derived Grad-Shafranov equation (GSE) is a highly non-linear partial differential equation and (while simply re-expressing the cross-field force balance) highlights that the structure of the magnetosphere essentially depends on the assumed field line rotation and the current distribution in the magnetosphere.[68,69] In the low inertia (high magnetization) limit and flat Minkowski space, the GSE (without differential rotation) reduces to the original pulsar equation and describes the solution of the time-independent set of FFE equations. An example of a possible magnetic field structure emerging from the disk is shown in Fig. 6.

Both, the FFE and the MHD fluid approach, essentially rely on the assumption that charge separation is/remains negligible everywhere such that $\vec{E} \cdot \vec{B} = 0$ is satisfied over the length scale of interest. This could be a reasonable assumption for e.g., field lines connecting to the disk and the surrounding plasma:

In the laboratory frame, the rotation of the magnetic field will induce an electric field $\vec{E} = -\vec{v}_{\rm rot}/c \times \vec{B}$. If not screened, this could in principle be tapped for the

---

[f]Defined in the non-relativistic case as the surface where the plasma kinetic energy density equals the magnetic field energy density. Relativistic flows remain Poynting-dominated at the Alfvén surface, with the Alfvén surface only being related to the propagation of Alfvén waves, that become static at this location.
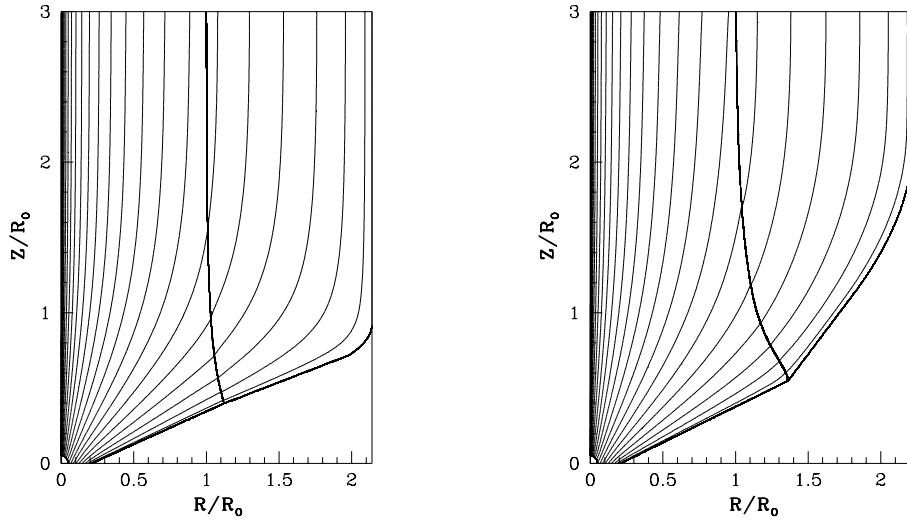
Fig. 6.   Poloidal magnetic field structure of a collimating, relativistic jet, obtained from the numerical solution of the stationary-state, axisymmetric relativistic MHD equations. The magnetosphere is assumed to be force-free. Dipolar magnetic flux carried by the accretion disk is stretched by a disk wind into the upper hemisphere. Left: Assuming weak differential (quasi-rigid) rotation of foot points of the field lines. Right: For strong differential rotation. R_0 denotes the asymptotic light cylinder radius. From Fendt and Memola[70].

acceleration of particles. By Gauss' law, the induced electric field is supported by a local charge density $\rho_e = \nabla \cdot \vec{E}/4\pi$, corresponding to a particle number density (commonly referred to as the Goldreich-Julian [GJ] density[71]) well inside r_{L} of

$$n_{\mathrm{GJ}} = \frac{\Omega B \cos\theta}{2\pi ec} = 0.1 \; \eta^{-1} \left(\frac{B}{10^4 \; \mathrm{G}}\right) \left(\frac{10^8 M_\odot}{M}\right) \; \cos\theta \; [\text{particles cm}^{-3}] \qquad (23)$$

where $\Omega = c/r_{\mathrm{L}}$, r_{L} is the typical light cylinder scale with $r_{\mathrm{L}} = \eta r_s$, and $\eta \sim (1-10)$ for disk and $\eta = 1/a \sim 1$ for (extreme) Kerr black hole magnetospheres. Here, θ denotes the field inclination. If the environment is plasma-rich ($n > n_{\mathrm{GJ}}$), the ability of charges to move freely along the field lines will ensure (at least inside r_{L}) that $\vec{E}\cdot\vec{B} \to 0$, i.e., the parallel electric field component essentially becomes screened. (As a natural consequence, gap-type particle acceleration in the induced electric field will be suppressed.) Applicability of the MHD approximation thus basically requires that the charge density is always larger than the critical Goldreich-Julian density. For self-consistency one may thus always wish to verify that this is satisfied within a numerically calculated flow.[72] The inner regions of AGNs are usually sufficiently plasma-rich to make this a useful working assumption for disk-driven outflows. If one conservatively assumes, for example, that accretion occurs close to the free fall timescale, i.e., $t_a \sim r/v_r$, $v_r \sim \alpha v_f$, $v_f = (GM/r)^{1/2}$, with α the viscosity parameter, the characteristic particle number density $n \sim \dot{M} t_a / \pi r^3 m_p$ close to r_s
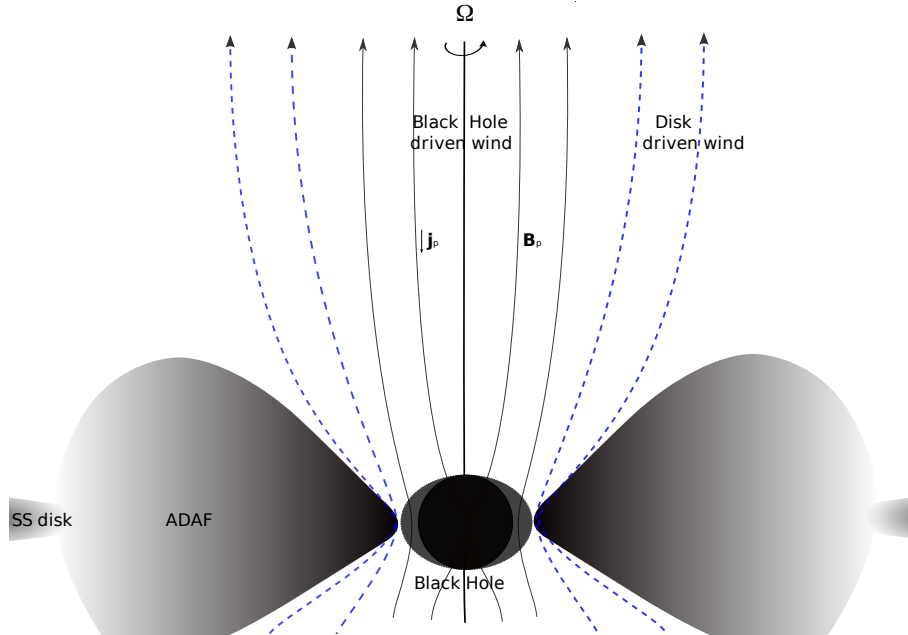
Fig. 7.   Schematic drawing of a possible field structure around a rotating black hole, with a black hole-driven wind surrounded by an outflow from the inner parts of the disk. The accretion flow may switch its configuration to a standard disk at some transition radius r_t.

becomes

$$n \sim 10^{12} \alpha^{-1} \left(\frac{\dot{M}}{\dot{M}_{\mathrm{Edd}}} \right) \left(\frac{10^8 M_\odot}{M} \right) \left(\frac{r_s}{r} \right)^{3/2} \; [\text{particles cm}^{-3}], \qquad (24)$$

i.e., orders of magnitude higher than the minimum GJ density required to screen the fields. The physical situation is less obvious for black hole-driven jets. Here, the nature of the plasma source that replenishes charges which escape the system along open magnetic field lines (both, outgoing to infinity and ingoing across the horizon) is less well understood, and charge-starved funnel regions or gaps can occur for which the ideal MHD description may not be adequate.[73,7] Plasma injection is then most likely be related to electron-positron pair production (cross-field diffusion being negligible), either due to direct $\gamma\gamma$-interactions of MeV photons in a hot accretion flow and/or initiated by, e.g., the Compton up-scattering of ambient photons by electrons/positrons accelerating in a vacuum gap (e.g.,refs.[60,74,75,21,76,77,7]). For a number of conditions, this is believed to ensure a plentiful supply of charges, cf. also eq. (68), so that the plasma around (e.g., above the gap) a "typical" AGN is commonly also considered to satisfy quasi-neutrality ($n^+ + n^- \gg n^- - n^+$).[78]

Global 3d-relativistic MHD simulations of black hole accretion disks and magnetospheres have in recent years benefited from a proliferation of numerical ap-

proaches.[g] The results are widely considered to answer, at least partially, some of the longstanding questions with respect to magnetically-dominated (Poynting-flux-dominated)[81] and matter-dominated jets.[33] Accordingly, the simulations confirm the general picture of a two-component sheath jet configuration with a fast, magnetically-dominated inner jet being surrounded by a slower moving, matter-dominated jet. As it appears, relativistic magnetically-dominated jets may in fact need an external agency (e.g. a disk wind) to facilitate efficient collimation (cf. also refs.[82,83]). There are indications that the jet formation process does not require ordered, large-scale magnetic fields to be fed in from larger disc scales,[81] and that the resultant outward-directed electromagnetic energy flux is consistent with the flux being powered by the Blandford-Znajek process.[84] The first point, however, may need some further confirmation as other simulations still seem to need large-scale seed fields (e.g., ref.[85]).

For the obtained matter-dominated jets, on the other hand, the main driving force seems to be a high-pressure corona (no evidence for the operation of a Blandford & Payne-type process has been found yet), where strong (gas plus magnetic) pressure gradients ensure that matter is pushed into the jet (leading to extended mass loading) and accelerated along it.[33] This comes along with relatively slow jet speeds ($\Gamma_j \sim 1.5$) and large opening angles.

While very instructive, these global simulation results still face (apart from the usual methodological constraints, see e.g., ref.[86]) a number of limitations whose influences need to be carefully assessed in order to allow detailed contact with observations. Among others, this relates to the facts that: (i) Not all of the global numerical schemes employed are fully conservative (e.g., in Hawley et al. only the internal, but not the total energy is explicitly conserved). (ii) Radiation fields, although observationally important, are as yet not fully included (e.g., in McKinney). This could obviously modify the flow dynamics and considerably influence the heating and cooling of the plasma. In fact, it has been argued that for powerful quasar-type sources, radiative driving may play an important role in shaping the outflow.[87] (iii) Usually, the plasma content is assumed to be conserved, which may not be appropriate in the vicinity of the black hole, where pair creation is occurring all the time (e.g., refs.[62,7]). (iv) The results can depend strongly on the chosen initial and boundary conditions. Since magnetic fields are, e.g., divergence-free, they seem never able to fully forget their (artificial) initial configurations, making the resultant jets very sensitive to these (observationally poorly known) conditions.[88] (v) While global approaches rely on the ideal (infinite conductivity/zero resistivity) MHD limit, longterm simulation results seem to provide evidence for (artificial) reconnection-driven magnetic island formation. The occurrence of magnetic reconnection could significantly change the global field configuration and the plasma dynamics[89] (for an illustration of the role of finite resistivity in the Newtonian

---

[g]The interested reader is referred to the relevant reviews by, e.g. Fragile[79] and Krolik & Hawley[80] for more details and references.

limit, see ref.[90]; for the special relativistic case see ref.[91]). It is not clear to which extent this might invalidate some of the numerical results obtained so far with ideal MHD.

Nevertheless, for the purpose of our investigation here, we may visualize a simplified field structure as shown in Fig. 7.

3. PARTICLE ACCELERATION IN BLACK HOLE-JET MAGNETOSPHERES

3.1. *Direct electric field acceleration and the Blandford-Znajek process*

A black hole embedded in an external poloidal field B_p and rotating with angular velocity $\Omega_H = a(c/2r_H)$, Eq. (6), will induce an electric field of magnitude $|\vec{E}| \sim (\Omega_H r_H)B_p/c$ corresponding to a permanent voltage drop across the horizon of magnitude $\Phi \sim r_H|\vec{E}| = (a/2)r_H B_p$. In terms of the electric circuit analogy, a black hole can act like a unipolar inductor (battery) with non-zero resistance, so that power can be extracted by currents flowing between its equator and poles. For reasonable astrophysical parameters, the potential drop (noting that one statvolt [cgs] corresponds to 300 V [SI]) is of order (cf. ref.[20])

$$\Phi \sim 2 \times 10^{19} \, a \, (1 + \sqrt{1 - a^2}) \left(\frac{M}{10^8 M_\odot} \right) \left(\frac{B_p}{10^4 \text{ G}} \right) \text{ [V]} \qquad (25)$$

If a charged particle can fully tap this potential, acceleration up to ultra-high energies of $E = Ze\Phi \sim 3 \times 10^{19} Z(M/10^8 M_\odot)(B_p/10^4 \text{ G})$ eV may become possible. Rapidly spinning and massive black holes have thus often been considered as astrophysical candidates for the energization of UHE cosmic rays (cf. § 5.2.2). As noted above, however, the charge density in the vicinity of accreting black holes may well be so high that a significant fraction of this potential is screened and thus no longer available for particle acceleration (see, however, also ref.[92]). It seems thus more appropriate to define an effective potential where the available length scale (gap height h) is explicitly taken into account, i.e.,

$$\Phi_e \sim \Omega_H \left(\frac{h}{r_H} \right)^2 r_H^2 B_p/c = \left(\frac{h}{r_H} \right)^2 \Phi \,. \qquad (26)$$

Accordingly, the characteristic rate of energy gain can be expressed as

$$\frac{dE}{dt} = Ze\Phi_e c/h \,, \qquad (27)$$

with corresponding acceleration timescale $t_{\text{acc}} = \gamma m_0 ch/(Ze\Phi_e)$.
Equation (25) yields a strong electromotive force (EMF) which in the Blandford-Znajek (BZ) scenario is assumed to drive electric currents along the fields and to generate a power output $P_{\text{BZ}} = \Phi I = \Phi^2/(\Delta Z_s)$. As the event horizon does not have perfect conductivity but instead acts like free space with respect to the propagation of electromagnetic waves, its surface resistivity Z_s corresponds to the impedance of

free space (377 Ohm $= 4\pi/c$ [stat-ohm], with c in cgs).[93,20] Thus, if current closure can be achieved in the black hole environment (for field lines emerging between pole and equator, i.e. with resistance $\Delta Z_s \sim Z_s/4 \sim 100$ Ohm), a considerable electromagnetic (Poynting-flux-driven) power output of the order

$$P_{\mathrm{BZ}} \simeq 5 \times 10^{43} a^2 (1 + \sqrt{1-a^2})^2 k \left(\frac{M}{10^8 M_\odot}\right)^2 \left(\frac{B_p}{10^4 \ \mathrm{G}}\right)^2 \ \mathrm{erg/s}. \qquad (28)$$

might be generated, where a is the dimensionless spin parameter and $k \sim 1$ is a numerical factor accounting for the field geometry. To support such an electromagnetic power output, however, an electric current $I = (P_{\mathrm{BZ}}/\Delta Z_s)^{1/2} \sim 7 \times 10^{26}$statampere $\simeq 2 \times 10^{17}$A must flow within the magnetosphere, requiring a minimum steady pair injection (creation) rate of $dN_e/dt = I/Q \sim 10^{36}$ particles/s. The implied (minimum) particle number density would then be close to the Goldreich-Julian density estimated in eq. (23). Even if one neglects cross-field diffusion, this density could, as shown later on, most likely be maintained by pair creation alone, cf. eq. (68).

The above analysis, when put on a more rigorous basis (cf. the "Membrane paradigm"[20]), reveals a number of subtleties that have been the center of much attention and debate. To mention a few:

(1) In reality, the BZ power depends on the assumed magnetic field topology. The angular velocity of the field lines Ω_f, for example, does not simply coincide with the angular velocity of the black hole Ω_H, but is instead dependent on the global field structure. Even if the impedance-matched case (where the resistance of the BH "battery" equals the one of the "load" at large distances, i.e., where $\Omega_f = \Omega_H/2$) becomes established with time such that maximum power extraction is ensured,[94] the numerical factor k might well be smaller than one (e.g., $k \leq 0.2$ for a homogeneous magnetic field, see ref.[95]). In general, for an Eddington-limited system, the BZ process cannot extract energy at a rate much larger than $0.29 \, L_{\mathrm{Edd}}/\eta$, where $\eta \sim 0.1$ in the canonical conversion efficiency (cf. eq. [8]; also refs.[96,97]). Recent studies of powerful FR II radio galaxies suggest that these sources can have jet powers comparable to the accretion power $P \sim \dot{M}c^2$ (e.g., ref.[98]). This is much higher than expected from current, global relativistic MHD simulations of the BZ-process, that start off from a no-net-magnetic flux configuration, and may indicate that large-scale magnetic flux needs to be accreted in order for the process to operate efficiently enough (see ref.[99] for details).

(2) The "membrane" analogy, according to which the black hole horizon can be regarded as unipolar inductor with non-zero resistivity, has been fundamentally criticized on physical grounds[100] (cf. also ref.[101] for a response). As the horizon is causally disconnected from the external space and the outgoing flow, it actually cannot act as a unipolar inductor, which has led to general doubts concerning the nature of the BZ process. There are at least two (related) responses to this problem: (i) First, within the Grad-Shafranov MHD approach it can be shown that the "boundary condition" determining the potential energy loss of a rotating black hole

is in fact dictated by the physical parameters in the pair creation region outside and not at the horizon.[95,103] This gives about the same power output and illustrates that the nature of the BZ process does not have to rely on a questionable causal connection between the event horizon and the outer magnetosphere. (ii) Secondly, the physical source of the BZ process does not – when correctly interpreted – lie with the horizon itself, but with the ergosphere. As plasma is unavoidable forced into co-rotation within the ergosphere, the magnetic field (assumed to be frozen in the plasma) is forced into co-rotation as well. While the horizon is indeed causally disconnected from the outgoing wind, the ergosphere is not and the BZ mechanism can still be recovered.[102,104]

(3) In the BZ scenario, black holes are assumed to be surrounded by plenty of charges, ensuring that an electric current can flow along the poloidal magnetic fields. This poloidal current then results from the screening of the vacuum electric field. On the other hand, to sustain a stationary current, the electric field should retain small unscreened components and not become completely screened by a re-distribution of electric charges. Otherwise, the magnetospheres would no longer be able to drive electric currents (cf. ref.[100]). As it turns out, however, such a final state appears not possible within the ergosphere of a rotating black hole:[102] The electric field, which is induced "gravitationally", cannot become completely screened by any static distribution of electric charges, i.e., rotating black holes do not allow stationary solutions with completely screened electric fields and vanishing poloidal currents.

(4) The BZ process of extracting the rotational energy of black holes appears to be very similar, but not simply equivalent to the mechanical Penrose process.[105] Because plasma entering the ergosphere is forced to co-rotate with the black hole, magnetic field lines penetrating the ergosphere will get twisted by the differential rotation of the plasma. This twist of magnetic field lines propagates outwards along the field lines (against the infalling plasma flow) as a torsional Alfvén wave, establishing an outgoing electromagnetic energy flux. The magnetic tension of the bent field lines, on the other hand, decelerates the plasma in the ergosphere, imparting opposite angular momentum. The ergospheric plasma thus moves to lower energy orbits and the total (hydro- and electrodynamic) energy-at-infinity quickly decreases to negative values.[106] While it seems that initially the resultant Penrose energy extraction process essentially operates via negative hydrodynamic energy-at-infinity, longterm simulations suggest that regions of negative hydrodynamic energy-at-infinity eventually disappear, with the electromagnetic BZ process still continuing.[107] A more general analysis suggests, however, that the condition, for which the direction of the Poynting energy flux (at infinity) is opposite to that of the (local) field flow, is not simply equivalent to the Penrose one for negative energy-at-infinity (see, e.g. [108] for more details).

(5) According to recent results based on general relativistic MHD simulations, the maximum BZ jet power appears to be sensitive to the assumed jet-disk geometry. In the presence of, e.g., a thick disk (with effective thickness $(H/R) \sim 1$) the jet

power may actually scale more strongly with black hole spin, i.e., $P_{\mathrm{BZ}} \propto a^4$ instead of $P_{\mathrm{BZ}} \propto a^2$ for a thin disk.[109] If this is confirmed by further research, it may offer important clues for understanding the radio-loud/radio-quiet dichotomy in AGN.

3.2. *Direct electric field acceleration close to the light cylinder*

In early applications of the BZ process, charged particles (electric currents) are considered being able to cross the field lines only in the "load" region far away from the black hole.[110] Accordingly one may expect significant particle acceleration to occur mainly within that region. However, this needs not necessarily to be the case as has been demonstrated for pulsar magnetospheres:[111] Within ideal MHD, the structure of the magnetosphere is essentially determined by the supposed field line rotation and the assumed electric current distribution (cf. § 2.5). If the longitudinal electric current would become sufficiently small, the freezing-in condition will break down so that electrons, deviating from the field line, may become able to sample the full induced electric field and thereby get efficiently accelerated along the z-axis close to the black hole.[112] This would obviously allow acceleration beyond the asymptotic flow speed in ideal MHD $\gamma \sim \sigma_m^{1/3}$ (e.g., ref.[113]). As shown by Beskin & Rafikov[111] for a quasi-monopole magnetic field configuration, this could happen in a narrow boundary layer of thickness Δr close to the generalized light surface

$$r_{ls} = \frac{r_{\mathrm{L}}}{(2\eta_c)^{1/4}} \,, \tag{29}$$

where $|\vec{E}| = |\frac{\vec{v}_{\mathrm{rot}}}{c} \times \vec{B}| \simeq |\vec{B}|$. Here, $\eta_c > 0$ characterizes the strength of the longitudinal current in terms of the Goldreich-Julian current, $j_{\parallel} = (1 - \eta_c) j_{\mathrm{GJ}}$. For small longitudinal currents, i.e. $\eta_c \to 1$, the light surface coincides with the classical light cylinder

$$r_{ls} \to r_{\mathrm{L}} = \frac{c}{\Omega} \,. \tag{30}$$

Sampling an electric field of strength $\sim |\vec{B}|$, electron acceleration (in the absence of losses) is then approximately described by

$$\frac{d\gamma}{dr} \simeq \frac{eB}{m_e c^2} \tag{31}$$

The maximum electron Lorentz factor that can be achieved in the boundary layer of width Δr thus becomes

$$\gamma \sim \frac{d\gamma}{dr} \, \Delta r \,. \tag{32}$$

As the thickness of the layer depends on the charge density, i.e.,

$$\Delta r \sim \frac{r_{\mathrm{L}}}{\lambda} \,, \tag{33}$$

where $\lambda = n_e / n_{\mathrm{GJ}} \gg 1$ is the multiplicity factor and $n_{\mathrm{GJ}} = \Omega B / (2\pi c e)$ the Goldreich-Julian density,[111] the maximum Lorentz factor becomes

$$\gamma \sim \sigma_m \tag{34}$$

where $\sigma_m = B^2/(8\pi n_e m_e c^2)$ is the Michel[114] magnetization parameter. Thus, in a narrow boundary layer close to the light cylinder $r_{\rm L}$ almost all of the electromagnetic energy may be transformed into the kinetic energy of particles.

3.3. *Centrifugal acceleration close to the light cylinder*

A somewhat different approach, that does not rely on direct electric field acceleration but takes inertial (centrifugal) and radiation reaction effects explicitly into account, has been explored in the literature as well.[115,116,117,118,119,120,6,121]
This approach assumes that the plasma density is in fact high enough to ensure that the parallel electric field component is effectively screened out up to distances (of at least) very close to the light cylinder, and that the magnetic field structure is such as to allow a significant fraction of the electromagnetic energy to be transformed into the kinetic energy of particles through magneto-centrifugal effects close to $r_{\rm L}$. This goes along with the requirement that the longitudinal electric current is small enough. Consider for illustration a charged test particle, co-rotating with the magnetic field and gaining energy while moving outwards. Under most circumstances, an energetic electron will quickly lose its perpendicular energy component due to strong synchrotron losses and may thus be considered as just sliding along the field line. The motion of such a particle along a field line may be conveniently analyzed in the framework of Hamiltonian dynamics: The Lagrangian L for a particle with rest mass m_0 moving along a (two-dimensional) relativistically rotating field line (angular velocity $\Omega = c/r_{\rm L} = $ const.) is simply given by

$$L = -m_0 c^2 (1 - v_r^2/c^2 - v_\phi^2/c^2)^{1/2}. \tag{35}$$

where $v_r = \dot{r}$ and $v_\phi = \Omega r + \dot{r}\frac{B_\phi}{B_r}$ (note, that as the field is considered to be swept back, $B_\phi/B_r < 0$). As L is not explicitly time-dependent, the Hamiltonian $H = \dot{r}P - L$, with $P = \partial L/\partial \dot{r}$ the generalized momentum, is a constant of motion (Noether's theorem). Using the above relations, one easily finds (cf. also ref.[122])

$$H = \gamma m_0 c^2 \left(1 - \frac{\Omega r}{c^2} v_\phi \right) = {\rm const.}, \tag{36}$$

where $\gamma = (1 - v_r^2/c^2 - v_\phi^2/c^2)^{-1/2}$ is the Lorentz factor of the particle. This can be generalized to the case where $\vec{B}$ and $\vec{\Omega}$ are inclined at an angle θ by replacing $r \to (r\sin\theta)$ on the rhs of eq. (36) and, correspondingly, in Ferraro's law of isorotation. Note that the above expression might have also been obtained from the standard Bernoulli equation (energy flow conservation). Provided the product $\dot{r}B_\phi/B_r$ remains sufficiently small, this implies

$$\gamma(r) \propto \frac{1}{(1 - r^2/r_{\rm L}^2)}. \tag{37}$$

Thus, for a particle approaching the light cylinder $r \to r_{\rm L}$, the Lorentz factor may increase dramatically as long as co-rotation holds. However, even in the single

particle approach the Lorentz factor cannot become arbitrarily large, as from a formal point of view the validity of the approach demands that at least $\omega_c \leq \Omega$ (see also the breakdown constraint below),[123] where $\omega_c = eB/(\gamma m_0 c)$ is the relativistic gyro-frequency. Using Eq. (36) and the definition of γ, the characteristic acceleration time scale can be expressed as[6]

$$t_{\mathrm{acc}} = \frac{\gamma}{\dot{\gamma}} \simeq \frac{1}{2\,\Omega\,\tilde{m}^{1/4}\gamma^{1/2}}\,, \tag{38}$$

valid for $\gamma \gg 1$, where $\tilde{m} = 1/(\gamma_0^2\,[1 - r_0^2/r_{\mathrm{L}}^2]^2)$ depends on the initial injection conditions. Under more realistic circumstances, achievable particle Lorentz factors are expected to be limited either (i) by radiative losses (curvature or Compton), (ii) by the breakdown of the (single particle) bead-on the wire approximation (relevant for, e.g., protons), or (iii) - if we consider an ensemble of particles - by the particles' inertia overcoming the tension in the field lines (i.e., breakdown of plasma co-rotation, e.g., see ref.[124]). In the simplest case the breakdown (ii) corresponds to the situation where the Coriolis force becomes comparable to the Lorentz force. It is tantamount to requiring that the inverse of the relativistic gyro-frequency ω_c remains smaller than the acceleration timescale.[121] This translates into an upper limit on achievable Lorentz factors of

$$\gamma_{\mathrm{max}} \simeq 2 \times 10^8\,\tilde{m}^{-1/6} \left(\frac{B(r_{\mathrm{L}})}{100\ \mathrm{G}}\right)^{2/3} \left(\frac{m_e}{m_0}\right)^{2/3} \left(\frac{r_{\mathrm{L}}}{10^{14}\mathrm{cm}}\right)^{2/3} \tag{39}$$

where $B(r_{\mathrm{L}})$ denotes the field strength at the light cylinder r_{L}.

3.4. *Magnetic reconnection at the jet base*

Efficient magnetic reconnection (annihilation of magnetic fields) could possibly take place close to the black hole if there are suitable field regions with opposite polarities. In the reconnection process, the energy stored in these fields is released as kinetic energy and heat (increase in entropy) (cf. ref.[125] for review). This requires finite resistivity (i.e., breakdown of ideal MHD and the frozen-in condition) and becomes important in regions with large magnetic field gradients (for application to AGN see, e.g., refs.[126,127]). By Ampere's law, $\nabla \times \vec{B} = (4\pi/c)\vec{j}$, these large field gradients are associated with large current densities $\vec{j}$ ("current sheets"). Thus, even for a relatively high electrical conductivity σ_e, significant ohmic losses (j^2/σ_e) might occur.

The rate of magnetic reconnection is controlled by the geometry of the dissipation region. In the simplest (Sweet-Parker) picture, see Fig. 8, the inflow of plasma and magnetic field into the reconnection region at speed v_r is balanced by an outflow at speed v_A. The characteristic outflow speed for a magnetized plasma is the Alfvén speed $v_A = B/(4\pi n_c m_p)^{1/2}$. Mass conservation approximately implies $L\,v_r \sim dR\,v_A$, i.e., $v_r \sim (dR/L)v_A$. From the (steady state) induction e quation, the width can be estimated to be $dR \sim \lambda_m/v_r$, where $\lambda_m = c^2/(4\pi\sigma_e) \propto 1/R_m$ is the magnetic diffusivity ($R_m \sim v_A L/\lambda_m \gg 1$ the magnetic Reynolds number),

24   *F.M. Rieger*

measuring the ability of a magnetic field to diffuse through a plasma. This combines to $v_r \sim v_A/R_m^{1/2} \ll v_A$, so that the reconnection process would only proceed at very slow speeds, the classical problem associated with (Sweet-Parker-type) reconnection.

However, plasma micro-turbulence or wave-particle interactions might lead to an enhanced ("anomalous") resistivity (increasing λ), allowing faster reconnection rates with $v_r \to v_A$. Such a situation has been envisaged to take place at the interface between a black hole magnetosphere and a coronal wind, where poloidal magnetic field reversal may occur, see Fig. 8.[128,129] The maximum rate of magnetic energy
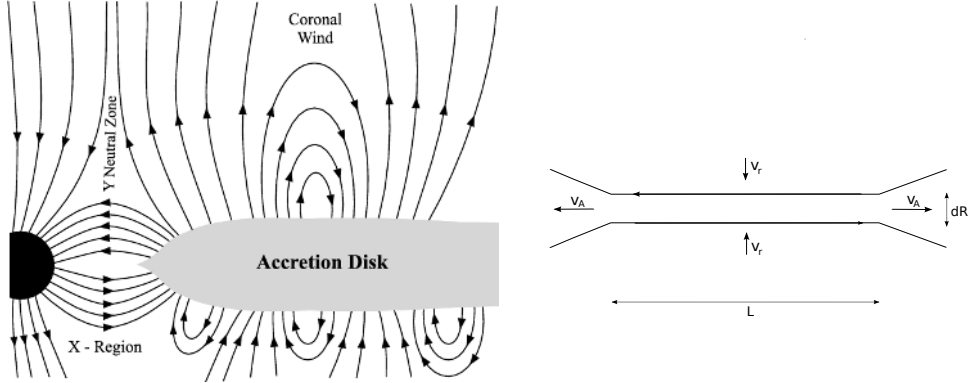

Fig. 8.   Left: Schematic drawing of the assumed magnetic field geometry. Acceleration could occur in the magnetic reconnection region at the Y-type neutral zone. From de Gouveia Dal Pino and Lazarian[128]. Right: Illustration of a simple reconnection region. Two oppositely directed magnetic fields in a plasma are carried towards the neutral line at speed v_r over a characteristic length scale L. There is a layer of width dR in which the field reconnects. Reconnected field and plasma are expelled at speed v_A.

that can be extracted from the reconnection zone in the corona (above and below the disk) would then be on the order of

$$P_B \sim (B^2/8\pi)v_r(4\pi R)L \sim (B^2/8\pi)v_A(4\pi R)dR \,, \tag{40}$$

where B is the magnetic field at the reconnection zone, $R \sim R_s$ is of the order of the inner radius of the disk, and $v_A \sim c$ for a highly magnetized plasma. In analogy to Ampere's law, we can roughly estimate the width dR of the current sheet for which the resistivity must be anomalous[128]

$$dR \sim \frac{c\Delta B}{4\pi n_c Ze v_{\mathrm{th,c}}} \sim 200 \, \frac{m_p c^2}{ZeB} \,, \tag{41}$$

where $v_{\mathrm{th,c}} \simeq (kT/m_p)^{1/2} \sim c/100$ is the typical thermal velocity of the ions in the X-ray ($kT \sim 100$ keV) emitting corona, and where $\Delta B \sim 2B \sim 10^5 \, (10^8 M_\odot/M)^{1/2}$ G (cf. § 2.4) denotes the change of the magnetic field across the reconnection region.

This gives a relatively modest power of

$$P_B \sim 5 \times 10^{37} \left(\frac{M}{10^8 M_\odot} \right)^{1/2} \text{ erg/s} . \tag{42}$$

Yet, while not sufficient to account for radio-loud AGNs, this power could perhaps be sufficient to explain the observed radio luminosities of radio-quiet AGNs (see Fig. 3 in ref.[129]).

During the reconnection process, efficient acceleration of supra-thermal particles in the inductive electric field $\vec{E}_r = \vec{v}_r \times \vec{B}/c$ perpendicular to the (two-dimensional) reconnection fields can occur as long as their Larmor radii do not exceed the width of the current sheet.[126] Ignoring energy losses, this would suggest that in the considered scenario (cf. eq. [41]) relativistic energies up to $\gamma_p \sim 2 \times 10^2$ (protons) and $\gamma_e \sim 4 \times 10^5$ (electrons) might become achievable (cf. also ref.[128] for possibility of further acceleration).

The details of the motion of charged particles in current sheets are non-trivial,[130] and obtained results are dependent on the (time-dependent) sheet structure and, e.g., the strength of the linking magnetic field perpendicular to the sheet. Possible particle spectra discussed in the literature for fast magnetic reconnection include quasi-monoenergetic distributions (e.g., ref.[131]) and power-law particle spectra $n(\gamma) \propto \gamma^{-s}$ with $s \simeq 1$ (e.g., ref.[132]) or $s \simeq 1.5$ (ref.[133]).

4. RADIATIVE PROCESSES

The interactions of energetic particles with (photon or magnetic) fields and/or ambient matter usually provide important efficiency constraints for the above mentioned acceleration mechanisms. Some of these loss processes and their possible relevance are discussed below.

4.1. *Synchrotron Radiation*

A charged particle with Lorentz factor γ and charge number Z spiraling in a magnetic field $\vec{B}$ emits synchrotron radiation with a mean frequency

$$\langle \nu \rangle = 0.31 \, \nu_{cs} \tag{43}$$

where $\nu_{cs} = (3/4\pi)\Omega_e \gamma^2 \sin\theta$, $\Omega_e = ZeB/(m_0 c)$ is the gyro-frequency and θ the pitch angle between the magnetic field and the velocity vector. The energy loss rate, $-dE/dt$, or the power emitted by a single particle is

$$P_{cs} = \frac{2}{3} \frac{Z^4 e^4}{m_0^2 c^3} \gamma^2 B^2 \sin^2\theta , \tag{44}$$

so that the characteristic cooling timescale $t_s = E/|dE/dt| = \gamma m_0 c^2/P_{cs}$ becomes

$$t_s = \frac{3 \, m_0^3 c^5}{2 \, Z^4 e^4 \gamma B^2 \sin^2\theta} \simeq 520 \left(\frac{m_0}{m_e} \right)^3 \left(\frac{10^3 \text{G}}{B} \right)^2 \frac{1}{Z^4 \gamma \sin^2\theta} \text{ sec} . \tag{45}$$

In terms of the mean frequency $\langle \nu \rangle$, one obtains

$$t_s \simeq 5.9 \times 10^{11} Z^{-7/2} (m_0/m_e)^{5/2} (B \sin\theta)^{-3/2} \langle \nu \rangle^{-1/2} \ \sec. \qquad (46)$$

The characteristic cooling time of a proton, for example, emitting synchrotron radiation at $\langle \nu \rangle = 2.4 \times 10^{26}$ Hz (energy of 1 TeV) is thus of order $t_s \simeq 64 \, (B \sin\theta)^{-3/2}$d. The synchrotron spectrum (power per unit frequency) $I(\nu)$ emitted by a single particle is a power law $I(\nu) \propto \nu^{1/3}$ for $\nu \ll \nu_{cs}$, and decreases exponentially for $\nu \gg \nu_c$. For most practical purposes, it can be reasonably approximated by $I(\nu) \propto (\nu/\nu_{cs})^{0.3} \exp(-\nu/\nu_{cs})$.

Equation (45) shows that for almost all pitch angles θ, energetic electrons are expected to quickly radiate away their perpendicular momentum components in the strong magnetic fields close to the black hole. Electrons in the black hole magnetosphere may thus be regarded as mainly occupying the ground ($n = 0$) Landau state, moving quasi-one-dimensionally along the field lines. In order to emit synchrotron radiation, particles in the ground Landau state would have to be excited to higher Landau levels (by acquiring non-vanishing pitch angles). This is not excluded but may become possible through, e.g., Compton scattering or non-resonant diffusion in pitch angles.[134,135,136]

4.2. *Curvature Radiation*

In the black hole magnetosphere, and in particular closer to the light surface, the curvature of the magnetic field may no longer be negligible, so that particles moving along the fields might efficiently lose energy due to curvature radiation. In analogy to synchrotron radiation, curvature radiation can be described as emission from relativistic charged particles moving around the arc of a circle chosen such that the actual acceleration corresponds to the centripetal one, i.e. with curvature radius $R_c = \gamma m_0 c^2 / (ZeB \sin\theta)$ (e.g., ref.[137]). The critical frequency where most of the radiation is emitted is given by

$$\nu_c \simeq \frac{3c}{4\pi R_c} \gamma^3 \,, \qquad (47)$$

which for a curvature radius of, e.g. $R_c = r_s = 3 \times 10^{13} (M/10^8 M_\odot)$ cm yields $\nu_c \simeq 2 \times 10^{26} \, (\gamma/10^{10})^3$ Hz or a curvature photon energy of about $1 \, (\gamma/10^{10})^3$ TeV. Like synchrotron emission, the spectrum $I(\nu)$ produced by curvature radiation of a single particle is a power law $I(\nu) \propto \nu^{1/3}$ for $\nu \ll \nu_c$, and decreases exponentially for $\nu \gg \nu_c$. The energy loss rate or total power radiated away by a single particle (charge number Z) is

$$P_c = \frac{2}{3} \frac{Z^2 e^2 c}{R_c^2} \gamma^4 \,. \qquad (48)$$

The characteristic cooling timescale $t_c = \gamma m_0 c^2 / P_c$ thus becomes

$$t_c \simeq 180 \frac{R_c^2}{Z^2} \left(\frac{m_0}{m_e} \right) \frac{1}{\gamma^3} \,. \qquad (49)$$

In the absence of other damping mechanisms, a balance with cooling $dE/dt = P_c$ (using eq. [27]) would imply that direct electric field acceleration may account for particle Lorentz factors up to (cf. ref.[138])

$$\gamma_{c,\mathrm{max}} \simeq 10^{10} \, \frac{a^{1/4}}{Z^{1/4}} \left(\frac{M}{10^8 M_\odot} \right)^{1/2} \left(\frac{B_p}{10^4 \mathrm{G}} \right)^{1/4} \left(\frac{R_c}{r_H} \right)^{1/2} \left(\frac{h}{r_H} \right)^{1/4} , \qquad (50)$$

provided the potential (gap height h, spin a, cf. eqs. [25,26]) is such that these Lorentz factors can in principle be achieved. Note that eq. (50) does not depend on the particle (e.g., electron or proton) mass. The maximum energy of the emitted curvature photons becomes

$$\epsilon_c = \frac{3}{2} \frac{c\hbar\gamma_{c,\mathrm{max}}^3}{R_c} \simeq 2 \, a^{3/4} \left(\frac{M}{10^8 M_\odot} \right)^{1/2} \left(\frac{B_p}{10^4 \mathrm{G}} \right)^{3/4} \left(\frac{R_c}{r_H} \right)^{1/2} \left(\frac{h}{r_H} \right)^{3/4} \mathrm{TeV} .$$
$$(51)$$

Equation (50) suggests that the maximum energy for a charged particle of mass μm_p may exceed $\sim 10^{19}\mu$ eV only in massive black hole environments. The magnetic field strength typically scales as $B \propto M^{-1/2}$ (cf. § 2.4), so that efficient UHE proton acceleration would require a very massive source. Equation (51) then suggests that this should be accompanied by significant VHE γ-ray emission.

As an illustration, let us suppose that particles are efficiently accelerated in the magnetosphere of a massive black hole, with their maximum energies only limited by curvature losses. As noted above, this could lead to detectable emission in the TeV energy band. For the gap to exist, the charge density has to be smaller than the Goldreich-Julian value, cf. eq. (23), i.e., $n \le n_{\mathrm{GJ}} = \Omega B/(2\pi e c)$ (provided this density can be supported by the fields). Assuming a quasi mono-energetic particle distribution, the total curvature output at energy ϵ_c, eq. (51), is then of order $L_c \simeq n \, \Delta V \, P_c$. If acceleration takes place in a gap (of thickness h, with associated volume element $\Delta V \sim \pi\eta r_g^2 h$, where $\eta \le 1$ is a geometrical factor), we have at maximum $P_c = dE/dt = e\Phi_e c/h$ (cf. eq. [27]). This would imply a maximum VHE luminosity of the order of (e.g., [7])

$$L_c \simeq n \, (\pi\eta r_g^2 h) \left(\frac{e\Phi_e c}{h} \right) \qquad (52)$$
$$\simeq 8 \times 10^{43} \eta \left(\frac{n}{n_{\mathrm{GJ}}} \right) \left(\frac{B}{10^4 \mathrm{G}} \right)^2 \left(\frac{M}{10^8 M_\odot} \right)^2 \left(\frac{h}{r_g} \right)^2 \frac{\mathrm{erg}}{\mathrm{s}} .$$

It is interesting to note that the ratio L_c/P_{BZ}, where P_{BZ} denotes the maximum Blandford-Znajek power, eq. (28), scales as $(h/r_g)^2$ (see also ref.[7]).

4.3. *Inverse Compton Scattering*

Compton scattering of photons by relativistic electrons (Lorentz factor $\gamma \gg 1$) is usually called inverse Compton (IC) scattering. The IC power for single scattering of an isotropic photon distribution with energy density $U_{\mathrm{ph}} \simeq h \int_0^{m_e c^2/\gamma h} d\nu \, \nu n_{\mathrm{ph}}(\nu)$

28   *F.M. Rieger*

[erg/cm^3] in the Thomson limit $h\nu \ll m_e c^2/\gamma$ (i.e., for negligible energy transfer in the electron rest frame) is

$$P_{\rm IC} = -\frac{dE}{dt} = \frac{4}{3}\sigma_T c\gamma^2 U_{\rm ph}\,, \qquad (53)$$

which gives a characteristic electron cooling timescale of

$$t_{\rm IC} \simeq 3.1 \times 10^7 \frac{1}{\gamma U_{\rm ph}}\ {\rm sec}\,. \qquad (54)$$

The photon scattering rate, i.e., the total number of incident and up-scattered photons per unit time is $c\sigma_T n_{\rm ph}$, where $n_{\rm ph} = U_{\rm ph}/h\,\langle\nu\rangle$. From $P_c = c\sigma_T n_{\rm ph} h\,\langle\nu_1\rangle$ one deduces that the mean scattered photon frequency is

$$\langle\nu_1\rangle = \frac{4}{3}\gamma^2\,\langle\nu\rangle \qquad (55)$$

where $\langle\nu\rangle$ is the average incident photon frequency. From the kinematics, the maximum (peak) photon energy after scattering is $\nu_1 = 4\gamma^2\nu$ for radiation with incident frequency ν. Taking the Thomson condition into account, we have $h\nu_1 \sim \gamma m_e c^2$. If Compton recoil cannot be neglected (i.e., if the Thomson regime does not apply), the full Klein-Nishina cross-section must be used, resulting in a reduced power output. Based on QED considerations, the total cross-section is given by the Klein-Nishina (KN) formula, for which two useful limits are

$$\sigma \simeq \sigma_T \quad \text{for } h\nu_r \ll m_e c^2$$
$$\simeq \frac{3}{8}\sigma_T \left(\frac{m_e c^2}{h\nu_r}\right)\left[\ln\left(\frac{2h\nu_r}{m_e c^2}\right) + \frac{1}{2}\right] \quad \text{for } h\nu_r \gg m_e c^2\,. \qquad (56)$$

where ν_r is measured in the rest frame of the electron. In the extreme KN regime, the energy loss rate for a single electron is found to be[139]

$$-\frac{dE}{dt} \simeq \frac{3}{8}\sigma_T m_e^2 c^5 h^{-1} \int_{m_e c^2/\gamma h}^{\infty} d\nu\ \frac{n_{\rm ph}(\nu)}{\nu}\left[\ln\left(\frac{4\gamma h\nu}{m_e c^2} - \frac{11}{6}\right)\right]\,, \qquad (57)$$

and is thus only weakly (logarithmically) dependent on the electron Lorentz factor γ. However, in contrast to the Thomson case, the photon now carries away a sizable fraction of the electron energy, so that the electron loses its energy in discrete steps. The spectrum emerging from single inverse Compton scattering generally depends on both, the seed photon spectrum and the relativistic electron distribution. If the range of the seed photon spectrum is very narrow compared to the electron distribution (assumed to obey a power-law $n_e(\gamma) \propto \gamma^{-s}$ between $\gamma_{\min}$ and $\gamma_{\max}$), for example, the output spectrum is a power-law $\nu^{-(s-1)/2}$ over a dynamical range of $(\gamma_{\max}/\gamma_{\min})^2$, with index determined by the electron power-law index. On the other hand, if the electron distribution is very narrow compared to the photon distribution, the output spectrum resembles the seed photon spectrum shifted in energy by a factor $\sim \langle\gamma^2\rangle$.

If electrons are rotationally accelerated in the magnetosphere of a black hole embedded in an ambient photon field, Compton losses may significantly reduce achievable

particle energies. In the Thomson regime, for example, inverse Compton upscattering of accretion disk photons will lead to particle energy losses on a timescale $t_{\rm IC} \propto \gamma^{-1}$ that decreases faster than $t_{\rm acc} \propto \gamma^{-1/2}$, eq. (38), and so introduces a natural limitation. Balancing acceleration by cooling, eq. (54), implies a characteristic upper limit of (e.g., ref.[120])

$$\gamma_{\rm max} \sim 3 \times 10^6 \, \frac{\sqrt{\tilde{m}}}{U_{\rm ph}^2} \left(\frac{10^{15} {\rm cm}}{r_{\rm L}} \right)^2 , \tag{58}$$

assuming co-rotation to hold for such a range of Lorentz factors. Hence, only for highly underluminous AGN sources with target photon fields $L_t \ll L_{\rm Edd}$ ($U_{\rm ph} \sim L_t/[4\pi r_{\rm L}^2 c]$), will centrifugal acceleration allow to accelerate electrons to Lorentz factors $\gamma \gg 100$.[118,119]

4.4. *Photo-meson production*

Photo-meson production can become an important channel by which the kinetic energy of protons is transformed into high energy gamma-rays, electrons and neutrinos.[140] The kinematic threshold for single pion production (p+$\gamma \rightarrow p + \pi^0, n + \pi^+$) is given by

$$2 E_p \epsilon_\gamma (1 - \cos\theta) = (2 m_\pi m_p + m_\pi^2) c^4 \simeq 2.8 \times 10^{17} \ ({\rm eV})^2 \tag{59}$$

where E_p is the proton energy (assumed to be relativistic), $\epsilon_\gamma = h\nu$ is the target photon energy and m_π the pion rest mass. Thus, in the rest frame of the proton, the photon energy has to exceed $\epsilon_\gamma' = m_\pi c^2 (1 + m_\pi/2 m_p) \simeq 140$ MeV for the process to become possible. Close to the energy threshold, the process proceeds through single-pion production, while at higher energies multi-pion production channels start to dominate. The cross-sections for these inelastic processes are known from particle acceleration experiments. In first-order approximation, they can be expressed as a sum of two step-functions with $\sigma_1 = 0.34$ mbarn ($= 3.4 \times 10^{-28}$ cm^2) in the interval 200 MeV $\leq \epsilon_\gamma' \leq 500$ MeV and $\sigma_2 = 0.12$ mbarn for $\epsilon_\gamma' \geq 500$ MeV, and related inelasticities $K_{p,1} = 0.2$ and $K_{p,2} = 0.6$, respectively.[141] For the characteristic attenuation length we have $\lambda \sim 1/(n_\gamma \sigma K_p)$, where n_γ is the photon number density [particles/cm^3], so that the characteristic proton cooling time $t_{\rm c} = \lambda/c$ becomes

$$t_{\rm c} \sim \frac{5 \times 10^{17} {\rm sec}}{n_\gamma} \sim 3 \times 10^6 \left(\frac{\epsilon_\gamma}{1 \ {\rm keV}} \right) \left(\frac{10^{42} {\rm erg/s}}{L} \right) \left(\frac{R}{10^{14} {\rm cm}} \right)^2 \ {\rm sec} , \tag{60}$$

where $n_\gamma \simeq L/(4\pi R^2 c \epsilon_\gamma)$ has been expressed in terms of the source luminosity L. If the inner disk surrounding the black hole would be of the standard (geometrically-thin, optically-thick) type, then the thermal disk radiation field would be dominated by emission from regions close to r_s, with energy peaking at $\epsilon_\gamma \sim 50$ eV, cf. eq. (15), and thereby provide a suitable ambient target field for protons with Lorentz factors above $\gamma_{p,t} \sim 2 \times 10^6$ (50 eV/ϵ_γ). Neglecting curvature losses and field screening, gap-type particle acceleration of protons up to ultra-high energies $\sim 10^{20}$ eV, cf. eq. (26),

would then only be possible if mass accretion occurs at low rates corresponding to disk luminosities $L_d \stackrel{<}{\sim} 0.01 L_{\text{Edd}}$ (cf. ref.[142]).

4.5. *Bethe-Heitler (proton-photon) pair production*

At energies below the threshold for photo-meson production, the main channel for inelastic interactions of energetic protons with ambient photons is the direct production of electron-positron pairs, i.e. the process $p+\gamma \to e^+ + e^- + p$, e.g.refs.[140,143] The minimum energy (threshold condition) required for this process to become possible is

$$\gamma_p \epsilon_\gamma (1 - \beta_p \cos\theta) \geq 2 \left(m_e c^2 + \frac{m_e}{m_p} m_e c^2 \right), \tag{61}$$

where $\gamma_p = E_p/m_p c^2$ is the proton Lorentz factor and ϵ_γ the ambient photon energy. Thus, for head-on collisions the process is energetically allowed when $\gamma_p \epsilon_\gamma > m_e c^2$. The maximum energy of the resultant electron (positron) is determined by the kinematics and (for $m_e c^2 \ll \gamma_p \epsilon_\gamma \ll m_p c^2$) given by (cf. inverse Compton scattering) $E_{e,\max} = 4\gamma_p^2 \epsilon_f$. The cross-section for this process (often referred to as Bethe-Heitler cross-section) is about two orders of magnitude higher than the one for photo-meson production, but on average only a small fraction of the proton energy ($\sim m_e/m_p$) is lost. This is different to photo-meson production, where a proton transfers on average $\sim 13\%$ and more of its energy to the secondary products. As a consequence, photo-meson production usually becomes the dominant energy loss channel above the threshold eq. (59).

A variant of the Bethe-Heitler pair production process in the ergosphere of a maximally rotating, supermassive black hole (referred to as Penrose Pair Production) has been suggested already some 30 years ago as an efficient way for energy extraction from rotating Kerr black holes:[144,145] Upon entering the ergosphere, photons with energies of some tens of MeV (as might be produced in a hot ADAF inner disk via decay of neutral pions from pp-collisions, ref.[146]) could get boosted (blue-shifted) by a factor of up to ~ 30 (for extreme Kerr black holes) and so approach GeV energies. These photons could then interact with the (low-energy) protons moving on marginally stable orbits deep within the ergosphere to produce electron-positron pairs. From the threshold condition, minimum photon energies of only $2m_e c^2$ would be required. However, in order to become a Penrose Process, the recoiling protons must be injected on negative energy orbits (and pass through the event horizon), with the escaping pairs ejected with an energy boost picked up from the rotational energy of the Kerr black hole. Kinematically this requires the blue-shifted photon to have an energy comparable to the rest mass energy of the proton, giving GeV energies to the escaping electron-positron pairs. While this process may in principle be possible, detailed Monte Carlo simulations suggest it to be less important as most of the pairs apparently do not manage to escape.[147]

4.6. *Inelastic proton-proton collisions*

Relativistic protons and nuclei can produce high energy gamma-rays in inelastic collisions with ambient gas.[148] The neutral π^0-meson (with main $\simeq 99\%$ decay mode into two photons, e.g., $p+p \to p+p+\pi^0$, $\pi^0 \to 2\gamma$) provides the main channel of conversion of kinetic energy to high energy gamma-rays. For π^0-production to become kinematically possible, the kinetic energy of the bombarding proton must exceed $E_{\mathrm{th}} = 2m_\pi c^2(1 + m_\pi/[4m_p]) \simeq 280$ MeV. The cross-section and the inelasticity for pp-collisions both depend weekly on the energy, i.e., $\sigma_{pp} \simeq 3.4 \times 10^{-26}$ cm^2 and total inelasticity $f_\pi \simeq 0.5$. The characteristic cooling timescale $t_{pp} \sim 1/(\sigma_{pp} n_p f_\pi c)$ for a relativistic proton thus becomes

$$t_{pp} \sim 2 \times 10^7 \left(\frac{10^8 \mathrm{cm}^{-3}}{n_p}\right) \mathrm{sec}\,, \tag{62}$$

where n_p is the ambient gas density. While t_{pp} is only weakly dependent on the energy of the proton, the cooling timescale for $p\gamma$-reactions, cf. eq. (60), is expected to decrease with (increasing) proton energy (i.e., lower photon energy). Under such conditions, pp-interactions can dominate the cooling only below a certain proton energy (cf. also ref.[149] for an application to AGN).

In the simple delta-functional approximation,[150] the neutral pion takes away a mean fraction $f_{\pi^0} \simeq 0.17$ of the kinetic energy of the proton $E_{\pi^0} = f_{\pi^0} E_{\mathrm{p,kin}}$, and this energy is equally distributed among its decay products. The shape of the photon spectrum is then similar to the shape of the parent proton spectrum, but shifted in energy by a factor f_{π^0}.

4.7. $\gamma\gamma$-*Absorption*

Photon-photon interactions can produce electron-positron pairs $(\gamma + \gamma \to e^+ + e^-)$ and thereby lead to a suppression of the VHE photon flux from a source, once the kinematic threshold condition for pair production $(h\nu)(h\nu_t) > 2(m_e c^2)^2/(1 - \cos\alpha)$ is satisfied (α being the angle between the incident directions of the photons). TeV photons, for example, can thus react (head-on) with infrared target photons of energy $\epsilon_t = h\nu_t \sim 0.3$ eV. The electron-positron pairs produced in energetic collisions will be highly relativistic and tend to move in the direction of the initial VHE γ-ray.

For a fixed photon energy ϵ, the pair-production cross-section $\sigma_{\gamma\gamma}$ is a function of target energy ϵ_t:[151] If we denote by $s = E^2/(4m_e^2 c^4)$ the normalized centre-of-mass energy of the photons squared ($E^2 = 2\epsilon\epsilon_t[1 - \cos\alpha]$), then starting from zero at the threshold energy $s = 1$, the cross-section rises steeply to a maximum $\simeq (\sigma_T/4)$ at $s \simeq 2$ and decreases approximately $\propto 1/s \propto 1/\epsilon_t$ towards higher energies, i.e.,

$$\sigma_{\gamma\gamma}(s) \simeq \frac{3}{8}\frac{\sigma_T}{s}\left[\ln(4s) - 1\right] \tag{63}$$

32   *F.M. Rieger*

for $s \gg 1$. In an isotropic background radiation field, TeV photons thus interact most efficiently with infrared target photons of energy

$$\epsilon_t \simeq 1 \left(\frac{1\,\mathrm{TeV}}{\epsilon} \right) \ \mathrm{eV} \,. \tag{64}$$

The optical depth, characterizing the absorption of a γ-ray with energy ϵ moving through a target photon gas of spectral and spatial distribution $n(r, \epsilon_t)$ in a source of size R, can then be calculated from

$$\tau(\epsilon) = \int_0^R dr \int_{2(m_e c^2)^2/[\epsilon(1-\cos\alpha)]}^{\infty} d\epsilon_t \ n_\gamma(r, \epsilon_t) \ \sigma_{\gamma\gamma}(\epsilon, \epsilon_t, \alpha) \ (1-\cos\alpha) \,. \tag{65}$$

For a homogeneous source and a quasi-isotropic target photon field, the optical depth becomes[h]

$$\tau(\epsilon) \simeq R \int_{2(m_e c^2)^2/\epsilon}^{\infty} d\epsilon_t \ n_\gamma(\epsilon_t) \ \bar{\sigma}_{\gamma\gamma} \,, \tag{66}$$

where $n_\gamma(\epsilon_t)$ is the differential target photon number density. Because the optical depth for a gamma-ray of energy ϵ is essentially determined by a relatively narrow band of target photons (centered at $s = 2$), a useful order-of magnitude estimate is given by $\tau(\epsilon) \simeq 2.5(\sigma_T/4)R\epsilon_t n_\gamma(2\epsilon_t)$.[153] In terms of the luminosity L_t above energy $\epsilon_t \propto 1/\epsilon$, the optical depth may thus be approximated by

$$\tau(\epsilon) \simeq \frac{5\sigma_T L_t}{128\pi R c \epsilon_t} \simeq 0.3 \left(\frac{L_t}{10^{40}\,\mathrm{erg/s}} \right) \left(\frac{10^{16}\,\mathrm{cm}}{R} \right) \left(\frac{\epsilon}{1\,\mathrm{TeV}} \right) \,. \tag{67}$$

When applied to AGNs, this suggests that only in highly under-luminous ($L_t \ll L_{\mathrm{Edd}}$) and massive ($R \propto r_s \propto M$) sources, VHE gamma-rays may be able to escape unabsorbed from the vicinity of the central supermassive black hole. As an application, let us suppose that the inner accretion disk is of the high-temperature ($T_e \sim 5 \times 10^9$ K) ADAF type (see § 2.3.4). The dominant part of the radiation in the hard X-ray regime ($h\nu \sim kT_e \sim 500$ keV) would then be due to thermal bremsstrahlung. These hard X-ray photons would preferentially interact with target photons of energy $\epsilon_t \sim 2$ MeV (cf. eq. [64]). Although the disk spectrum would be suppressed at these energies (as the bremsstrahlung spectrum falls of exponentially with $\exp[-h\nu/kT_e]$), it may still be strong enough to lead to some non-negligible electron-positron pair production. We can roughly estimate the density of pairs so provided by balancing the rate of their creation with the rate of their escape:[i] The pair creation rate [particles/sec] is of the order of $\dot{N}_i \sim (4/3)\pi R^3 n_\gamma/t_{\mathrm{life}}$ where $t_{\mathrm{life}} \sim 1/(n_\gamma \sigma_{\gamma\gamma} c)$ is the characteristic lifetime of an incident photon. The created pairs will escape from the source region at a rate $\dot{N}_e \sim 4\pi R^2 n_e c$ (ignoring Compton

---

[h]A full analysis would have to employ the appropriate angle-averaged cross-section $\bar{\sigma}_{\gamma\gamma}$, see e.g. 152.

[i]I owe this argument to Marek Sikora.

scattering). Hence we find $n_e \sim n_\gamma^2 \sigma_{\gamma\gamma} R/3$. Using $n_\gamma \sim L_t/(4\pi R^2 c \epsilon_t)$, we have

$$n_e \sim \frac{L_t^2 \sigma_{\gamma\gamma}}{48\pi^2 R^3 c^2 \epsilon_t^2} \simeq 3 \left(\frac{L_t}{10^{40}\text{erg}} \right)^2 \left(\frac{10^{14}\text{cm}}{R} \right)^3 \left(\frac{2 \text{ MeV}}{\epsilon_t} \right)^2 \text{ [particles cm}^{-3}\text{]}. \quad (68)$$

Given the conventional AGN parameter space, one may expect the so-estimated pair density to be comparable to the Goldreich-Julian density in a fair number of sources, implying that a substantial part of the parallel electric field in the magnetosphere may be screened. This may not be the case, however, for highly under-luminous systems such as M87 and Sgr A*.[7,77] In terms of the accretion rate, the density ratio of so-created pairs (in a two-temperature ADAF) to the GJ value approximately follows[7]

$$\frac{n_e}{n_{\text{GJ}}} \sim 10^{12} \dot{m}^{7/2} \left(\frac{M}{10^8 M_\odot} \right)^{1/2}. \quad (69)$$

Hence, if the accretion rate would become very small, an additional plasma source (such as cascade formation in starved magnetospheric regions) would be needed to establish a force-free outflow (where $n_e \geq n_{\text{GJ}}$).

Note that if a source is sufficiently compact, its VHE γ-ray emission could well be shaped by the development of an electromagnetic cascade (photo-production of pairs, subsequent inverse Compton scattering etc.).[154] Also, since both TeV $\gamma\gamma$-absorption and photo-meson production, § 4.4 can interact with similar target photon fields, TeV gamma-ray observations could constrain the photo-pion production opacity, in particular for sources where rapid VHE gamma-ray variability is observed. When applied to TeV blazars, this suggest that the expected flux of high energy neutrinos from $p\gamma$-interactions is much less than the observed VHE gamma-ray flux, making them less promising targets for neutrino observations.[155]

5. APPLICATIONS

5.1. *Low-luminous galactic nuclei*

According to the considerations above, nearby under-luminous and non-aligned 'active' galactic nuclei emerge as prime candidate sources where non-thermal VHE processes, occurring close to the central black hole, may become observable and thereby allow to probe the most violent region of the central engine: If the source is sufficiently *under-luminous*, VHE gamma-rays may be able to escape significant absorption. The source must then, however, be relatively *nearby* in order to be within the reach of current or upcoming telescope sensitivities. Finally, if the jet is sufficiently *misaligned*, the nearby black hole VHE emission may not be swamped by Doppler-boosted jet emission. This makes sources such as Sgr A* or the nearby radio-galaxies M87 and Cen A to interesting candidates.

5.1.1. *The galactic centre source Sgr A**

Given its proximity, the compact radio source Sgr A* in the central region of our Galaxy may represent the most promising target for studying particle acceleration processes near the event horizon of a supermassive black hole. Believed to host a black hole of mass $M_{\rm BH} \simeq (3-4) \times 10^6 M_\odot$,[14] its extraordinary low bolometric luminosity ($\leq 10^{-8} L_{\rm Edd}$) is expected to make the innermost region transparent to γ-rays with energies up to ~ 10 TeV.[156] Estimates for the accretion rate in Sgr A* are in the range $\dot{M} \simeq (0.1-4) \times 10^{-6} M_\odot/\mathrm{yr}$,[157,158,159] so that $\dot{m} = \dot{M}/\dot{M}_{\rm Edd} \stackrel{<}{\sim} 5 \times 10^{-5}$. This suggests that the magnetic field in the innermost region could possibly be as high as $B \sim 5 \times 10^3$ G, cf. §2.4.

Early VHE observations of the Galactic Centre region by Imaging Atmospheric Cherenkov Telescopes have led to the detection of a steady, point-like source of VHE gamma-rays at the gravitational center of our Galaxy, coincident with the position of at least three counterparts, the supermassive black hole Sgr A*, the supernova remnant (SNR) Sgr A East (at a projected distance of 3.7 pc to Sgr A*), and the pulsar wind nebula G359.95-0.04 (at a projected distance of 0.4 pc to Sgr A*).[160,161,162,163,164] Recent H.E.S.S. results based on high precision pointing, however, now seem to exclude Sgr A East as the dominant source of the observed VHE gamma-rays.[165] On the other hand, both G359.95-0.04 and Sgr A* remain promising VHE counterpart candidates, as models exist that could explain the observed emission extending beyond 10 TeV (e.g., see ref.[166] for G359.95-0.04). In the case of Sgr A*, for example, the origin of the observed TeV emission has been related to (i) non-thermal processes in the black hole magnetosphere itself,[156] (ii) pp-interactions of escaping high energy protons in the surrounding dense gas environment,[167,168,169] or possibly (iii) electron acceleration in the termination shock of a wind emerging from the innermost parts of the disk.[170]

Suppose that particles could be efficiently accelerated in voltage gaps close to the black hole horizon. Then assuming a rapidly spinning black hole, eqs. (25) and (50) suggest that protons may possibly be able to reach energies up to $\simeq 10^{18}$ eV ($\gamma_p \sim 10^9$).[171] If so, then curvature emission is expected to peak around $\sim 10^{10}$ eV, eq. (47), i.e., well below the TeV domain. However, detectable TeV γ-ray emission may still be possible due to other radiative channels, and at least three different scenarios have been proposed:[156]

(1) *Photo-meson interactions:* If protons are able to reach energies of $\sim 10^{18}$ eV, they can start to interact with infrared soft photons, cf. eq. (59). Although the mid-to-near infrared source in Sgr A* is faint with $L_{\rm IR} \sim 10^{35}$ erg/s, it appears sufficiently compact $r_{\rm IR} \stackrel{<}{\sim} 10^{13}$ cm (e.g., refs.[172,173,174]) to ensure a high enough seed photon density $n_\gamma \sim (10^{12} - 10^{13})$ cm^{-3} for effective interactions with protons. The mean free path of protons through such a photon field, however, would be comparatively large, i.e., $\lambda \sim 1/(\sigma_{p\gamma} n_\gamma K_p) \sim (10^{15} - 10^{16})$ cm, cf. §4.4. This suggests that only a modest fraction $r_{\rm IR}/\lambda \leq 0.01$ of the energy in protons can be converted into secondary particles. Thus, in order to account for a VHE flux level

of $L_\gamma \sim 10^{35}$ erg/s,[160] an injection power up to $\sim 10^{38}$ erg/s in high energy protons would be required.

(2) *Proton-proton interactions:* If protons are not accelerated to energies $\sim 10^{18}$ eV in Sgr A* (as e.g. expected in the case of centrifugal acceleration), the efficiency of photo-meson interactions would be significantly reduced. Interactions of energetic protons with the ambient plasma could then become the main channel of VHE γ-ray production. The associated cooling time scale for pp-interactions is of order $t_{pp} \sim 2 \times 10^7$ $(10^8 \text{cm}^{-3}/n_p)$ sec, cf. eq. (62), for typical densities $n_p \sim (10^7 - 10^8)$ cm^{-3} in the inner regions of the accretion flow near Sgr A*, cf. eq (24). If the efficiency of gamma-ray production is determined by the ratio e_r of accretion time scale $t_a \sim r/v_r \sim 10^3$ sec (with $v_r \sim \alpha v_f$, v_f the free fall velocity) to cooling time scale,[156] then the efficiency of converting the energy of accelerated protons to secondaries may be as small as $e_r \sim 10^{-5}$. Hence, a high injection power of $L_\gamma/e_r \sim (10^{39} - 10^{40})$ erg/s would be required, very close to what may actually be provided by accretion.

(3) *Inverse Compton scenario:* Upscattering of soft photons by accelerated electrons may provide the most economic way to produce VHE γ-rays. If the infrared source represents the main target field, inverse Compton upscattering will proceed in the Klein-Nishina regime, requiring electrons energies $\overset{>}{\sim} 10$ TeV to account for the observed TeV emission. In order to avoid suppression by dominant electron synchrotron losses, particle acceleration must then essentially proceed along the ordered magnetic field. Both, centrifugal and/or gap-type particle acceleration are potential candidates to this end. If gap-type particle acceleration would be limited by curvature losses, for example, up-scattering could result in VHE γ-rays with energies $E_\gamma \sim \gamma_e m_e c^2 \sim (10^{14} - 10^{15})$ eV, cf. eq. (50). These energetic photons will, however, not be able to escape the source, but instead interact with far-infrared photons to produce electron-positron pairs. Synchrotron radiation and inverse Compton scattering by these secondary electrons will lead to a re-distribution of the initial gamma-ray spectrum. Figure 9 shows a model calculation of the expected spectral energy distribution within such a scenario.

5.1.2. *The radio-galaxy M87*

Located at a distance of $d \sim 16$ Mpc (redshift of $z = 0.0043$), the giant elliptical Virgo-cluster galaxy M87 represent another promising candidate for magnetospheric VHE γ-ray emission. M87 hosts one of the most massive black holes $M_{\rm BH} \simeq (3-6) \times 10^9 \, M_\odot$ in the Universe[175,176] and shows a prominent, non-aligned jet detectable from radio to X-ray wavelengths. Despite its huge black hole mass, M87 is not a powerful source of radiation: Based on its estimated total nuclear (disk and jet) bolometric luminosity of $L_{\rm bol} \sim 10^{42}$ erg/s or less,[177] M87 is highly underluminous with $l_e \le 3 \times 10^{-6}$, where $l_e = L_{\rm bol}/L_{\rm Edd}$ and $L_{\rm Edd}$ is the Eddington luminosity. This has led to the proposal that M87 is a prototype galaxy, where accretion occurs in an advective-dominated (ADAF) mode characterized by an in-
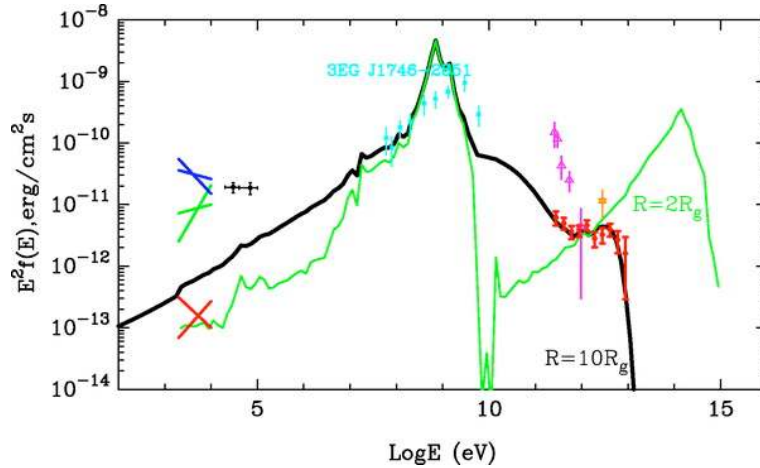
36   *F.M. Rieger*

Fig. 9.   Possible broadband SED for Sgr A* produced by electron curvature (1st peak) and inverse Compton (2nd peak) radiation. The thin solid line represents the gamma-ray spectrum due to the accelerated (primary) electrons, the thick solid line shows the redistribution of the energy after the passage through the infrared source. Figure adapted from Aharonian & Neronov[156] (reproduced by permission of the AAS).

trinsically low radiative efficiency.[178,179,180] HST observations of M87 have revealed superluminal motion of jet components at ~ 0.5 kpc from the central black hole, indicative of bulk flow Lorentz factors $\Gamma_b \sim 6$ and a jet orientation of $\theta \sim 19°$ to the line of sight (ref.[181]; see also ref.[182] for larger θ based on 43 GHz radio observations), suggesting that M87 is a non-blazar jet source, characterized by only moderate Doppler factors $D = 1/[\Gamma_b(1 - \beta\cos\theta)] \lesssim 3$.

Despite this, recent TeV observations[1,3,2] have demonstrated that the γ-ray spectrum of M87 extends beyond 10 TeV and is consistent with a relatively hard power-law (with spectral index $\alpha \sim 1.2$, where $S_\nu \propto \nu^{-\alpha}$), see Fig. 10. The TeV output is relatively moderate, with an isotropic TeV luminosity of some 10^{40} erg/s. Significant variability (flux doubling) on time scales of $\Delta t_{\rm obs} \simeq (1-2)$ days has been found, the fastest variability observed in any waveband from M87 so far. The observed spectral and temporary VHE γ-ray characteristics of M87 have been proven difficult to account for within classical jet models (cf. ref.[183] for review) and renewed the interest into magnetospheric emission models.[5,6,121,7] This interest has been strengthened by the recently detected correlation between radio VLBA (probing scales down to some tens of r_s) and TeV γ-ray data during a flaring state of M87 in 2008, see also Fig. 1.[4] There are also indications that a simple extrapolation of the Fermi (200 MeV–30 GeV) high energy spectrum under-produces the TeV flaring state,[184] supporting the possible appearance of a new (variable) component at the highest energies.

If the observed TeV emission would indeed be due to magnetospheric processes, one may expect the light travel time across the source of $\gtrsim 0.2$ days to provide a lower
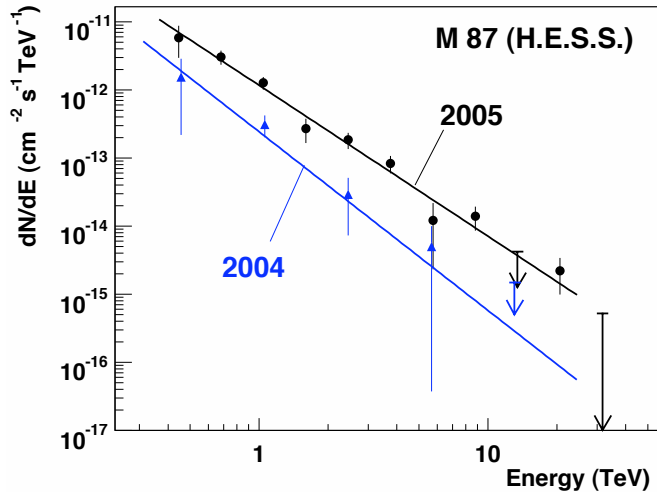
Fig. 10. The differential very high energy (VHE) spectra of M87 as obtained by H.E.S.S. during a low (in 2004) and a bright (in 2005) state, ranging from ~ 400 GeV to ~ 10 TeV. The indicated fits give power law photon indices of $(\alpha + 1) = 2.62 \pm 035$ (2004 data) and $(\alpha + 1) = 2.22 \pm 0.15$ (2005 data). No variation in spectral shape is found within errors. For comparison: One Crab unit at 1 TeV corresponds to a flux of $\simeq 3 \times 10^{-11}$ s^{-1} cm^{-2}. Figure from Aharonian et al.[1]

limit on the possible variability time scale at VHE energies. This is obviously close to what can be probed with existing Cherenkov arrays, and is certainly within the reach of future instruments like CTA. The observed day-scale variability already implies, e.g., that the (generalized) light surface, eq. (29), must be very close to the light cylinder scale of a few r_g, which in the direct acceleration model § 3.2 is equivalent to the requirement of a small longitudinal current. The observed, fast variability also excludes, e.g., pp-interactions as dominant channel for VHE γ-ray production in M87.

If the accretion rate in M87 is indeed of the order of the Bondi accretion rate $\dot{M} \sim 10^{-3}\dot{M}_{\rm Edd}$,[180] then possible magnetic field strengths in the vicinity of the black hole could be as high as $B \sim 1000$ G, see § 2.4. This would be consistent (if the black hole is sufficiently spinning) with poloidal magnetic field strengths required by a Blandford-Znajek-type process (eq. [28]) to account for the estimated jet kinetic power of a few 10^{44} erg/s.[185,177]

If electrons are centrifugally accelerated in an ambient photon field of order $L_{\rm bol}$, achievable particle energies may be as high as $\gamma_e \sim (10^7 - 10^8)$, cf. eq. (58). Similar (and most likely even higher) energies might be achievable if efficient gap-type particle acceleration would indeed take place, see eq. (27).[7] If the inner disk is of the ADAF-type, this could facilitate upscattering (Thomson regime) of (comptonized) sub-mm ADAF disk photons, i.e., those soft photons above the synchrotron peak $\nu_p \sim 10^{11}$ Hz, cf. eq. (20). Upscattering would results in emission at $\sim 5 \, (\gamma_e/10^7)$ TeV energies and can produce a hard photon spectrum close to what has actually

been observed.[121] If, on the other hand, the shape of ambient disk photon field would be more of the standard disk-type, then secondary inverse Compton cascade emission, initiated by internal absorption, could become influential at TeV energies as well.[5]

An important question for magnetospheric scenarios is whether TeV photons can escape from the vicinity of the central black hole. In principle, TeV photons of energy ϵ will interact most efficiently with target photons in the infrared regime $\epsilon_T \simeq (1\,\mathrm{TeV}/\epsilon)$ eV, eq. (64). The relevant infrared (IR) photon field needs thus to be sufficiently diluted in order to avoid significant pair-absorption. This could well happen if the IR emission is dominated by, e.g., emission from the jet (synchrotron emission) and/or a dusty torus on larger scales. For M87, the observed nuclear mid-infrared luminosity has been estimated to be $L_{\mathrm{IR}} \sim 10^{41}$ erg/s.[186] The corresponding optical depth for TeV photons would thus be $\tau \sim 3\,(10^{16}\mathrm{cm}/R_{\mathrm{IR}})$, eq. (67), assuming the infrared emission to be concentrated in a homogeneous source of size R_{IR}. Hence, for $R_{\mathrm{IR}} \sim$ some tens of r_s, TeV photons would be able to escape the source. This latter condition is probably difficult to satisfy for a standard-type disk where the emission from the innermost part is expected to peak close to the infrared regime, cf. § 2.3.2, but it seems well possible for a radiatively inefficient accretion flow. If one assumes, for example, that all of the observed nuclear radio to X-ray flux in M87 arises in an ADAF (which may appear over-restrictive given its jet), then ~ 10 TeV photons would have to be produced on scales $\gtrsim 5r_s$ (for a Kerr black hole) and $13r_s$ (for a non-rotating black hole) in order to be able to escape the source.[187] Recent findings, according to which the infrared emission is consistent with optically-thin synchrotron emission,[188] suggests that the real situation could be even more relaxed. Hence, there are good reasons to believe that, at least for M87, TeV γ-rays may be able to escape from the vicinity of its supermassive black hole.[7] This in turn suggests that future high-sensitivity instruments like the European CTA project could play a particularly important role in testing magnetospheric VHE γ-ray emission scenarios in M87.

5.1.3. *The radio-galaxy Cen A*

As the closest active galaxy (distance $d \sim 3.4$ Mpc, ref.[189]), the FR I source Centaurus A (Cen A, NGC 5128) seems another promising candidate worth exploring. Being a spectacular example of a gas-rich disk galaxy consumed in a merger with a giant elliptical galaxy, Cen A belongs to the best studied extragalactic objects (see, e.g., ref.[190]). Radio observations reveal a peculiar morphology with a sub-pc-scale jet and counter-jet, a one-sided kpc-jet, two radio lobes and extended diffusive emission. VLBI observations suggest that Cen A is a non-blazar source, its jet being inclined at a rather large viewing angle $i \gtrsim 50°$ and characterized by moderate bulk flow speeds $u_j \sim 0.5$ c.[191,192] Its central black hole mass has been inferred to be in the range $M_{\mathrm{BH}} = (0.5 - 3) \times 10^8 M_\odot$.[193,194]

With an estimated bolometric luminosity output of the order of $L_b \sim 10^{43}$ erg/s,[186]

Cen A is rather under-luminous (although not highly) and believed to be accreting at sub-Eddington rates $\dot{M} \sim 10^{-3}\dot{M}_{\mathrm{Edd}}$. The apparent lack of a big blue bump UV feature seems to indicate that its inner disk is not of the standard-type.[195] In fact, the disk contribution seems consistent with a hybrid disk configuration where a standard disk is truncated at r_t and replaced by an ADAF in the inner regions close to the central black hole (cf. refs.[196,197,198]). If the inner disk in Cen A would remain cooling-dominated (standard disk), magnetic field strengths close to the black hole of order $B \sim 2 \times 10^3$ G might be expected, cf. eq. (21). If the disk switches to a radiatively inefficient mode, the characteristic magnetic field strengths may be higher, possibly approaching $B \sim 10^4$ G if its black hole mass is at the lower mass end, see eq. (22).

The possible association of some of the Pierre Auger Observatory (PAO) measured UHECR events above 57 EeV with Cen A has recently triggered a number of studies analyzing the efficiency of cosmic-ray acceleration in Cen A.[199,200,201,202] Based on data up to August 2007, the PAO Collaboration initially reported evidence for an anisotropy at the 99% confidence level in the arrival directions of cosmic rays with energies above $\sim 6 \times 10^{19}$ eV.[203] The anisotropy was measured by the fraction of arrival directions that were less than $\sim 3°$ from the positions of nearby AGN (within 75 Mpc) from the VCV catalog. While that correlation has now decreased using the newly available (twice as large) data set, the updated analysis still suggests that a region of the sky around the position of Cen A has the largest excess of arrival directions relative to isotropic expectations.[204] If efficient UHE cosmic-ray acceleration would indeed take place in Cen A, this would seem to require the operation of an additional acceleration mechanism beyond gap-type particle acceleration, at least in the case of a proton-dominated composition.[202] For even in the ideal case where (i) the ordered poloidal field is assumed to be of the order $B \sim 10^4$ G, (ii) the black hole to be rapidly spinning $a \sim 1$, (iii) almost the full induced electric potential to be available for particle acceleration, and (iv) radiative constraints to be negligible, achievable cosmic ray energies are not expected to exceed $E \simeq 2 \times 10^{19} Z\, a\, (M/10^8 M_\odot)^{1/2}(\dot{M}/10^{-3}\dot{M}_{\mathrm{Edd}})^{1/2}$ eV by much, cf. eq. (25). Dropping (iv) by taking curvature losses into account would reduce achievable proton energies to $\sim 10^{19}$ eV, see eq. (50). If, on the other hand, a centrifugal-type acceleration mechanism would be operative, achievable energies may be even smaller, see eq. (39). Acceleration of protons to energies beyond a few times 10^{19} eV in regular magnetic fields close to the black hole would thus seem to be disfavored, even if Cen A was in the past in more active stage. The situation is much more relaxed in the case of heavier elements like iron nuclei, and this may perhaps be consistent with recent PAO indications for an increase of the average mass composition with rising energies up to $E \simeq 10^{19.6}$ eV.[205]

At γ-ray energies, Cen A is the only AGN of the non-blazar type detected at MeV (COMPTEL) and GeV (EGRET) energies. Its nuclear spectral energy distribution (SED), based on non-simultaneous data, appears to be composed of two peaks,

one reaching its maximum at several times 10^{13} Hz and one peaking around 0.1 MeV.[206,198] The SED below 1 GeV has been successfully modeled within a simple jet synchrotron self-Compton (SSC) framework, assuming Cen A to be a misaligned BL Lac object and its first SED peak to be due to synchrotron emission (ref.[206]; for an alternative interpretation, cf. ref.[207]). The detection of faint VHE γ-ray emission (integral flux of $\sim 1\%$ of the Crab Nebula above 250 GeV) up to ~ 5 TeV has been recently reported by the H.E.S.S. collaboration.[208] The VHE spectrum (from ~ 250 GeV to 5 TeV) can be described by a power law with spectral index $\alpha \simeq 1.7 \pm 0.5$. No significant variability has been found in the data set. At lower γ-ray energies (100 MeV to some tens of GeV), Fermi has recently also detected both the core and the giant radio lobes of Cen A.[209,210] As it appears, a single population of high energy particles seems unable to account for the core flux observed by Fermi and H.E.S.S. In fact, a simple extrapolation of the Fermi (power law) spectra would tend to under-predict the flux at TeV energies.[210,211] This could possibly indicate an additional contribution to the VHE domain beyond the conventional SSC jet emission, emerging at the highest energies. Obvious candidates within this context could be: (i) electron inverse-Compton (IC) emission powered by magnetospheric processes (centrifugal acceleration of electrons) in an ADAF environment,[202] (ii) IC pair cascade emission in the radiation field of a standard disk,[212] provided the magnetic field is weak enough for synchrotron cooling to be suppressed (cf. also ref.[213]), and (iii) hadronic (pγ) interactions in a standard-type disk environment, provided protons can achieve $\gtrsim 10^{19}$ eV.[214] These approaches are complementary in that the leptonic scenario (i) requires a rather low ambient IR photon field close to the central source, whereas the leptonic model (ii) or the hadronic model (iii) are dependent on rather large UV and/or IR background fields. An exemplary output of model (iii) is shown Fig. 11.

Let us suppose that TeV γ-rays could be indeed produced relatively close to the central black hole in Cen A. Then given its putatively small source scale and relatively high nuclear mid-infrared brightness (isotropic $\sim 6 \times 10^{41}$ erg/s at $h\nu \sim 0.15$ eV, with evidence for an exponential cut-off towards higher frequencies, see, e.g., refs.[186,198]), efficient escape of these VHE photons might appear much more challenging for Cen A than for M87, cf. eq.(67). However, most of the nuclear IR emission may well arise on larger scales (note that the mid-IR emission is unresolved on scales ~ 0.2 pc) and thereby allow sufficient dilution. In fact, the observed nuclear mid-IR emission is commonly believed not to be produced closed to the black hole, but to be dominated by a non-thermal (non-isotropic!) synchrotron jet component at a distance of $\gtrsim 0.03$ pc (cf. refs.[206,198,215]) and/or a (quasi-isotropic) dusty torus on scales ~ 0.1 pc or larger (refs.[186,216]). If this would be indeed the case, then photons with energies of a few to several TeV might be able to escape unabsorbed, while absorption features should become apparent towards higher energies. This could be tested with future high-sensitivity VHE γ-ray instruments and help to disentangle the site of the VHE γ-ray production and the origin of the observed nuclear mid-IR

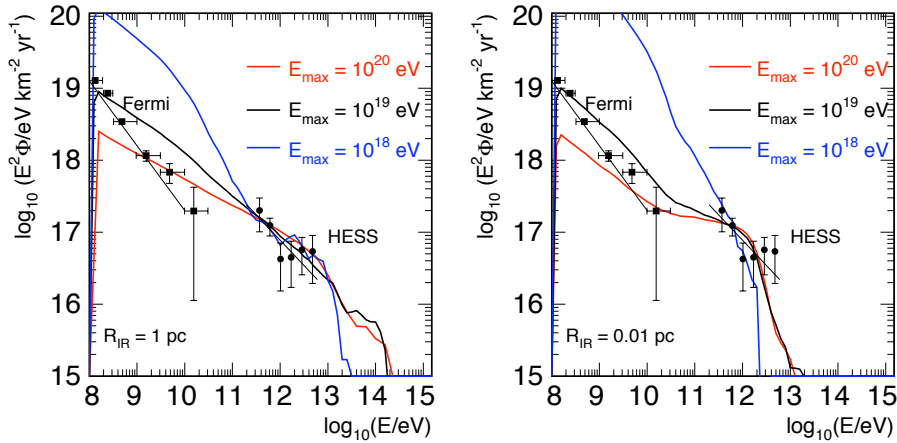Fig. 11.   Photon fluxes for Cen A calculated within a hadronic scenario, assuming pγ-interactions within a strong UV background photon field. Flux suppression by optical depth effects due to the ambient IR field becomes apparent towards higher energies. The different lines show the output for different maximum proton energies $E_{\max}$ assuming either a diffuse or compact IR source, i.e. a spatial IR source size of $R_{\mathrm{IR}} = 1$ pc and emission cut-off in far IR [left], or a source size 0.01 pc and no emission cut-off [right]. In order not to exceed the observed VHE fluxes, proton energies $\gtrsim 10^{19}$ eV seem to be required. Figure adapted from Kachelrieß et al.[214]

emission.

5.2. *Passive black holes as TeV γ-ray and UHE cosmic-ray sources*

If supermassive black holes would indeed be efficient UHE cosmic-ray accelerators, one may expect this to be accompanied by a significant TeV γ-ray output due to curvature radiation, e.g. ref.[217]. Observational constraints on the latter may then allow to impose physical constraints on the first. Perhaps the most obvious candidates for efficient gap-type particle acceleration are massive, but very weakly-emitting (dormant or "non-active") sources:

5.2.1. *The Fornax cluster galaxy NGC 1399*

Consider, for illustration, the giant elliptical Fornax cluster galaxy NGC 1399 at a distance of ~ 20 Mpc, already mentioned in § 2.1. Believed to host a supermassive black hole of mass $\sim 5 \times 10^8 M_\odot$,[17,218] it is well known for its low nuclear emissivity at all wavelengths. NGC 1399 exhibits weak FR I type radio activity (at a level of $\sim 10^{39}$ erg/s; see ref.[219]), but little evidence for significant non-thermal jet emission at higher energies. Based on an analysis of jet-induced cavities in the surrounding X-ray emitting medium on kpc-scale, a jet kinetic power of $P_{\mathrm{BZ}} \sim 10^{42}$ erg/s has been inferred.[220] If this jet power would be provided by a Blandford-Znajek-type (BZ) process, then ordered poloidal magnetic field strengths close to the black hole of the order of $B_p \sim 300/a$ G (with a the spin parameter) are to be expected, cf.

eq. (28).

Estimates for the (ADAF-type) accretion rate based on Chandra observations, on the other hand, seem to suggest $\dot{M} \sim 0.1\, \dot{M}_{\mathrm{Bondi}} \sim 2 \times 10^{-4} \dot{M}_{\mathrm{Edd}}$ (see refs.[221,222]) and would therefore imply (disk) magnetic field strengths (eq. [22]) $B_a \sim 10^3$ G, compatible with the one inferred from the observed jet power. Thus, if in addition the full electric potential would be available for particle acceleration (i.e., $a \sim 1$, $h \sim r_g$), electrons/protons might be able to reach maximum Lorentz factors $\sim 10^{10}$, i.e. protons may reach ultra-high energies of $\sim 10^{19}$ eV, cf. eqs. (25) and (50). This would yield curvature emission in the $\sim (0.1-1)$ TeV regime (eq. [51]). An important consequence of this is that a system containing a rapidly spinning black hole (such that it can be an efficient UHECR accelerator) should also emit curvature TeV photons, provided (i) vacuum breakdown does not occur and (ii) the TeV photons are able to escape.[138] In the case of NGC 1399 the later seems likely to be the case (cf. ref.[223]).

In order to sustain the observed BZ jet power, a current $I \simeq (P_{\mathrm{BZ}}/\Delta Z_s)^{1/2} \sim 10^{26}$ statampere $\simeq 3 \times 10^{16}$ A must flow through the magnetosphere. This would require an injection rate of $dN_e/dt \sim I/Q \sim 2 \times 10^{35}$ particles/s and imply a minimum charge density $n_e \sim N_e/V \sim (dN_e/dt)/(r_g^2 c) \sim 10^{-3}$ particles/cm^3. If this cannot be provided by annihilation of MeV disk photons, an additional plasma source would be needed to establish a BZ-type jet.

The accretion rate in NGC 1399 seems to be close to the critical value $\dot{m}_{\mathrm{crit}} \sim 3 \times 10^{-4}$ where annihilation of MeV photons in an ADAF could lead to an injection of seed charges of density n_e comparable to the Goldreich-Julian value $n_{\mathrm{GJ}} \simeq 7 \times 10^{-4}(B/300\mathrm{G})$ cm^{-3}, cf. ref.[7] If the accretion rate would be sufficiently high, i.e. $\dot{m} > \dot{m}_{\mathrm{crit}}$ ensuring $n_e > n_{\mathrm{GJ}}$, a substantial part of the electric potential may be screened (i.e., $h < r_g$ likely) so that efficient gap-type particle acceleration becomes suppressed. The anticipated curvature VHE output would be of the order of (cf. eq. [52]) $L_c \sim P_{\mathrm{BZ}} (h/r_g)^2$. For $(h/r_g)^2 \lesssim 0.1$, this would be consistent with the VHE upper limit $L_\gamma (> 200 \text{ GeV}) < 9.6 \times 10^{40}$ erg/s, imposed by H.E.S.S. observations of NGC 1399, see Fig. 12.[223] This would further reduce the available potential (eq. [26]), limiting achievable proton energies to $\ll 10^{19}$ eV. If, on the other hand, the accretion rate would be sufficiently small ($\dot{m} < \dot{m}_{\mathrm{crit}}$ implying $n_e < n_{\mathrm{GJ}}$), fully developed gaps ($h \sim r_g$) may exist, but an additional plasma source (such as cascade formation in starved magnetospheric regions, ref.[7]) would be needed to ensure a force-free outflow. The gap would then emit VHE γ-rays with a total luminosity of order $L_c \sim (n_e/n_{\mathrm{GJ}})\, P_{\mathrm{BZ}}$. For $(n/n_{\mathrm{GJ}}) < 0.1$ this would again be consistent with the VHE upper limits from H.E.S.S. and Fermi observations.

5.2.2. *Quasar remnants as UHECR accelerators*

Provided screening is not effective (and the spin parameter high enough), acceleration of cosmic-rays to energies $\geq 10^{19}$ eV may become possible. This could perhaps be the case in inactive quasar remnants, harboring rapidly spinning, supermassive
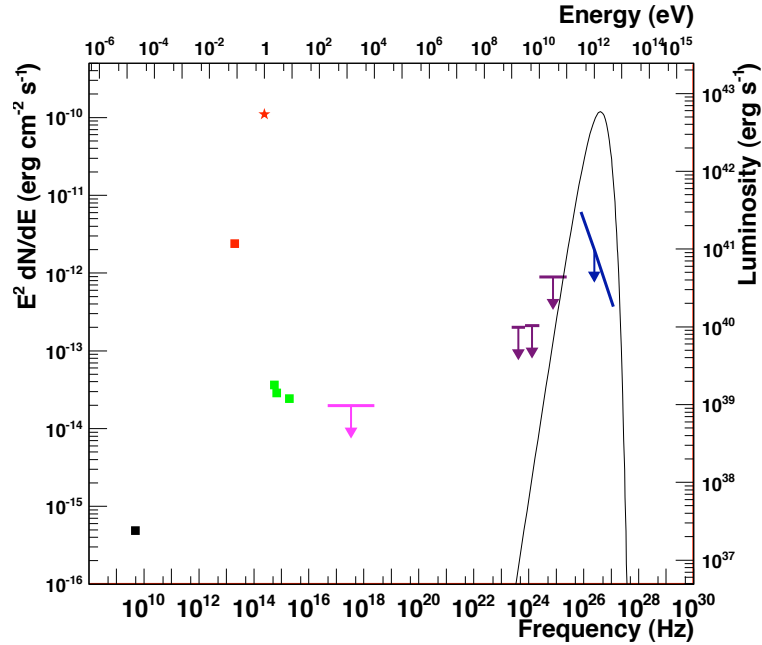
Fig. 12. The spectral energy distribution (SED) of NGC 1399, compiled from non-simultaneous public data (VLA radio, ISO IR, HST, Chandra, Fermi and HESS). Above the optical regime, only upper limits are available. The thin black line represents a toy curvature spectrum assuming a fully developed gap. Figure from Pedaletti et al.[223]

($> 10^9 M_\odot$) black holes.[224] The scenario envisaged is then one, where the black hole accelerator is not always operational in the normal, BZ-jet producing mode (associated with vacuum breakdown), but where (at least) sporadically the full gap size becomes available for the acceleration of a small number of protons. Primary target sources would thus be those that show little evidence for jets as well. While this may not work for NGC 1399 for reasons given above, Boldt & Ghosh[224] initially suggested a number of nearby massive dark objects that could potentially be efficient UHE ($\geq 10^{20}$ eV) proton accelerators. However, when curvature losses are fully accounted for,[138] most of these nearby sources turn out not to be capable of doing so, see eq. (50) (this seems also to apply to the revised list in ref.[225]). In fact, there is only a relatively small region of the parameter space (black hole mass, magnetic field strength) where one may expect proton acceleration to $\geq 10^{20}$ to be marginally possible. For this parameter region, however, the total power of the accompanying VHE radiation would appear to exceed the total power emitted in UHE cosmic rays by a factor of a hundred or more, making such hypothetical sources no longer quiescent in the TeV regime.[92] Given current evidence, it seems thus rather unlikely that (nearby) massive quasar remnants are promising candidates for efficient (gap-type) acceleration of protons to energies beyond 5×10^{19} eV, even if energy losses due to photo-pion production, cf. ref.[225], would be ne-

glected. As the constraint imposed by curvature losses is only mildly dependent on the charge number, heavier nuclei such as, e.g. iron Fe, might in contrast be able to reach energies $\gtrsim 5 \times 10^{20}$ eV in massive remnants. The propagation of such nuclei will, however, be significantly influenced by the interactions with the intergalactic radiation fields through photo-disintegration, with the particle being stripped from all its constituents nucleons after distances of a few Mpc only.[226,227]

6. Conclusions

Non-thermal processes occurring in the vicinity of supermassive black holes may allow new insights into the behavior of matter and energy under extreme conditions. The detection of, e.g., rapid variability on timescales of $\sim r_s/c$ and unusual high-energy emission signatures can provide an important diagnostic tool towards this end. Based on this, VHE observations during the last years have demonstrated the capacities of the new generation of VHE gamma-ray instruments (e.g., MAGIC II, HESS II, VERITAS and FERMI) to substantially improve our knowledge of the activity center in nearby, underluminous AGNs and to trigger new theoretical developments that could serve as benchmark for future VHE arrays like CTA. Detailed theoretical modelling of non-thermal particle acceleration and radiative numerical simulations may soon become indispensable in order to fully take advantage of the improved observational capacities.

Acknowledgement

References

1. F. Aharonian et al. (H.E.S.S. Collaboration), *Science* **314** (2006) 1424.
2. V.A. Acciari et al. (VERITAS Collaboration), *ApJ* **679** (2008) 397.
3. J. Albert et al. (MAGIC Collaboration), *ApJ* **685** (2008) L23.
4. V.A. Acciari et al. (VERITAS, MAGIC, VLBA M87 and H.E.S.S. Collab.), *Science* **325** (2009) 444.
5. A. Neronov and F.A. Aharonian, *ApJ* **671** (2007) 85.
6. F.M. Rieger and F.A. Aharonian, *A&A* **479** (2008a) L5.
7. A. Levinson and F. Rieger, *ApJ* **730** (2011) 123.
8. D. Richstone et al., *Nature* **395** (1998) 14.
9. M. Vika et al., *MNRAS* **400** (2009) 1451.
10. L. Ferrarese and H. Ford, *SSRv* **116** (2005) 523.
11. F. Shankar, *New Astronomy Reviews* **53** (2009) 57.
12. Ya.B. Zel'dovich and I.D. Novikov *Dokl. Acad. Nauk* **155** (1964) 1033.
13. R. Schödel et al., *Nature* **419** (2002) 694.
14. M.J. Reid, *IJMPD* **18** (2009) 889.
15. E. Tundo et al., *ApJ* **663** (2007) 53.

16. R. Falomo, J.K. Kotilainen and A. Treves, *ApJ* **569** (2002) L35.
17. R.C.W. Houghton et al., *MNRAS* **367** (2006) 2.
18. K. Gültekin et al., *ApJ* **698** (2009) 198.
19. D. Christodoulou, *Phys. Rev. Lett.* **25** (1970) 1596.
20. K.S. Thorne, R.H. Price and D.A. MacDonald, *Black Holes: The Membrane Paradigm* (Yale Univ. Press 1986).
21. B. Punsly, *ApJ* **498** (1998) 640.
22. R. Ruffini, G. Vereshchagin and S-S. Xue, *Physics Reports* **487** (2010) 140.
23. D.M. Eardley and W.H. Press, *ARA&A* **13** (1975) 381.
24. I.D. Novikov and V. P. Frolov, *Physics of Black Holes* (Kluwer Acad. Publ., 1989).
25. M. Volonteri et al., *ApJ* **620** (2005) 69.
26. E. Berti and M. Volonteri, *ApJ* **684** (2008) 822.
27. C.D.P. Lagos, N.D. Padilla and S.A. Cora, *MNRAS* **395** (2009) 625.
28. A. King, J.E. Pringle and J.A. Hofmann *MNRAS* **385** (2008) 1621.
29. J.M. Bardeen and J.A. Petterson, *ApJ* **195** (1975) L65.
30. K.S. Thorne, *ApJ* **191** (1974) 507.
31. J-M. Wang et al., *ApJ* **697** (2009) L141.
32. A. Martinez-Sansigre and A. Taylor, *ApJ* **692** (2009) 964.
33. J.F. Hawley and J.H. Krolik, *ApJ* **641** (2006) 103.
34. S.C. Noble, J.H. Krolik and J.F. Hawley, *ApJ* **692** (2009) 411.
35. C.S. Reynolds and M.A. Nowak, *Phys. Rep.* **377** (2003) 389.
36. L.W. Brenneman and C.S. Reynolds, *ApJ* **702** (2009) 1367.
37. S. Schmoll et al., *ApJ* **703** (2009) 2171.
38. G. Miniutti et al., *MNRAS* **398** (2009) 255.
39. A.S. Wilson and E.J.M. Colbert, *ApJ* **438** (1995) 62.
40. J.E. McClintock et al., *Classical and Quantum Gravity* (2011) to appear (arXiv:1101.0811).
41. R.P. Fender, E. Gallo and D. Russell, *MNRAS* **406** (2010) 406.
42. Q. Wu and X. Cao, *ApJ* **687** (2008) 156.
43. Q. Wu, X. Cao and D-W. Wang, *ApJ* (2011) in press (arXiv:1104.3235)
44. R. Daly, *MNRAS* (2011) in press (arXiv:1103.0940).
45. N.I. Shakura and R.A. Sunyaev, *A&A* **24** (1973) 337.
46. J.M. Bardeen, W.H. Press and S.A. Teukolsky, *ApJ* **178** (1972) 347.
47. S. Kato, J. Fukue and S. Mineshige, *Black Hole Accretion Disks* (Kyoto Univ. Press, 2008).
48. R. Narayan, R. Mahadevan and E. Quataert, in *Theory of Black Hole Accretion Disks*, ed. M.A. Abramowicz et al. (Cambridge Univ. Press), 148 (1998).
49. I. Yi, in *Astrophysical Disks*, ed. J. A. Sellwood, & J. Goodman, *ASP Conf. Ser.* 160 (1999) 279.
50. R. Mahadevan, *ApJ* **477** (1997) 585.
51. T. Manmoto et al., *ApJ* **489** (1997) 791.
52. R. Narayan and I. Yi, *ApJ* **428** (1994) L13.
53. R.D. Blandford and M.C. Begelman, *MNRAS* **303** (1999) L1.
54. I.V. Igumenshchev and M.A. Abramowicz, *ApJS* **130** (2000) 463.
55. M.A. Abramowicz, J.-P. Lasota and I.V. Igumenshchev, *MNRAS* **314** (2000) 775.
56. R. Turolla and C.P Dullemond, *ApJ* **531** (2000) L49.
57. M. Livio, G.I. Ogilvie and J.E. Pringle, *ApJ* **512** (1999) 100.
58. D.L. Meier, *New Astron. Rev.* **46** (2002) 247.
59. I. Contopoulos, D. Kazanas and D.M. Christodoulou, *ApJ* **652** (2006) 1451.
60. R.D. Blandford and R.L. Znajek, *MNRAS* **179** (1977) 433.

61. R.D. Blandford and D.G. Payne, *MNRAS* **199** (1982) 883.
62. R.D. Blandford, To the Lighthouse, in *Lighthouses of the Universe: Proceedings of the MPA/ESO/MPE/USM Joint Astronomy Conference*, eds. M. Gilfanov, R. Sunyaev, and E. Churazov (Springer, 2002), p. 381.
63. M. Camenzind, *Compact Objects in Astrophysics* (Springer, New York 2007).
64. S.S. Komissarov, *MNRAS* **336** (2002) 759.
65. X. Cao, *MNRAS* **291** (1997) 145.
66. M. Lyutikov, *MNRAS* **396** (2009) 1545.
67. A. Sadowski and M. Sikora, *A&A* **517** (2010) A18.
68. V.S. Beskin, *MHD Flows in Compact Astrophysical Objects* (Springer 2009).
69. I. Okamoto, *A&A* **326** (1997) 1277.
70. C. Fendt and E. Memola, *A&A* **365** (2001) 631.
71. P. Goldreich and W.H. Julian, *ApJ* **157** (1969) 869.
72. C. Fendt and R. Ouyed, *ApJ* **608** (2004) 378.
73. J.G. Kirk and I. Mochol, *ApJ* **729** (2011) 104.
74. M.J. Rees, *ARA&A* **22** (1984) 471.
75. V.S. Beskin, Y.N. Istomin and V.I. Parev, *SvA* **36** (1992) 642.
76. S. Vincent and S. Lebohec, *ApJ* **409** (2010) 1183.
77. M. Mościbrodzka et al., *ApJ* (2011) to appear (arXiv:1104.2042).
78. M.C. Begelman, R.D. Blandford and M.J. Rees, *Rev. Mod Phys.* **56** (1984) 255.
79. P.C. Fragile, *POS*(MQW7) (2008) 39.
80. J.H. Krolik and J.F. Hawley, *Lect. Notes Phys.* **794** (2010) 265.
81. J.C. McKinney, *MNRAS* **368** (2006) 1561.
82. C. Fendt, *ApJ* **651** (2006) 272.
83. S.S. Komissarov et al., *MNRAS* **374** (2007) 415.
84. J.C. McKinney and C.F. Gammie, *ApJ* **611** (2004) 977.
85. O. Porth and C. Fendt, *ApJ* **709** (2010) 1100.
86. G.K. Parks, *Space Sci. Reviews* **113** (2004) 97.
87. R. Kurosawa and D. Proga, *ApJ* **693** (2009) 1929.
88. K. Beckwith, J.F. Hawley and J.H. Krolik, *ApJ* **678** (2008) 1180.
89. S. Koide, *ApJ* **708** (2010) 1459.
90. C. Fendt, *ApJ* **692** (2009) 346.
91. C. Palenzuela et al., *MNRAS* **394** (2009) 1727.
92. A.Y. Neronov, D.V. Semikoz and I.I. Tkachev, *New Journal of Physics* **11** (2009) 065015.
93. T. Damour, *Phys. Rev. D.* **18** (1978) 3598.
94. S.S. Komissarov, *MNRAS* **326** (2001) L41.
95. V.S. Beskin and I.V. Kuznetsova, *IL Nuovo Cimento B* **115** (2000) 795.
96. G. Menon and C.D. Dermer, *ApJ* **635** (2005) 1197.
97. C.D. Dermer, J.D. Finke and G. Menon, *POS*(BLAZARS2008) (2008) 16 (arXiv:0810.1055).
98. C.A.C. Fernandes et al., *MNRAS* **411** (2011) 1909.
99. B. Punsly, *ApJ* **728** (2011) L17.
100. B. Punsly and F.V. Coroniti, *ApJ* **350** (1990) 518.
101. A. Levinson, *ApJ* **608** (2004) 411.
102. S.S. Komissarov, *MNRAS* **350** (2004) 427.
103. I. Okamoto, *PASJ* **58** (2006) 1047.
104. A. Levinson, in *Trends in Black Hole Research*, ed. P.V. Kreitler (Nova Science Publishers, 2006), p. 119.
105. R. Penrose, *Rev. Nuovo Cimento* **1** (1969) 252.

106. S. Koide, *Phys. Rev. D* **67** (2003) 104010.
107. S.S. Komissarov, *MNRAS* **359** (2005) 801.
108. S.S. Komissarov, *arXiv* (0804.1912) (2008).
109. A. Tchekhovskoy, R. Narayan and J.C. McKinney, *ApJ* **711** (2010) 50.
110. D. MacDonald and K.S. Thorne, *MNRAS* **198** (1982) 198.
111. V.S. Beskin and R.R. Rafikov, *MNRAS* **313** (2000) 433.
112. V.S. Beskin, A.V. Gurevich and Ya. N. Istomin, *ZhETF* **85** (1983) 401.
113. F.C. Michel, *Theory of Neutron Star Magnetospheres* (University of Chicago Press, 1991).
114. F.C. Michel, *ApJ* **158** (1969) 727.
115. G.Z. Machabeli and A.D. Rogava, *Phys. Rev. A* **50** (1994) 98.
116. G.Z. Machabeli, I.S. Nanobashvili and A.D. Rogava, *R&QE* **39** (1996) 26.
117. R.T. Gangadhara and H. Lesch, *A&A* **323** (1997), L45
118. F.M. Rieger and K. Mannheim, *A&A* **353** (2000) 473.
119. Y.D. Xu, *A&A* **381** (2002) 357.
120. Z. Osmanov, A. Rogava and G. Bodo, *A&A* **470** (2007) 395.
121. F.M. Rieger and F.A. Aharonian, *IJMPD* **17** (2008b) 1569.
122. I. Contopoulos, D. Kazanas and C. Fendt, *ApJ* **511** (1999) 351.
123. Y.N. Istomin and H. Sol, *Ap&SS* **321** (2009) 57.
124. Z. Osmanov and F.M. Rieger, *A&A* **502** (2009) 15.
125. E.G. Zweibel and M. Yamada, *ARA&A* **47** (2009) 291.
126. H. Lesch, *LNP* **377** (1991) 211.
127. J.G. Kirk, *Phys. Rev. Lett.* **92** (2004) 181101.
128. E.M. de Gouveia Dal Pino and A. Lazarian, *A&A* **441** (2005) 845.
129. E.M. de Gouveia Dal Pino, P.P. Piovezan and L.H.S. Kadowaki, *A&A* **518** (2010) 5.
130. I.J.D. Craig and Y.E. Litvinenko, *ApJ* **570** (2002) 387.
131. H. Lesch and M. Pohl, *A&A* **254** (1992) 29.
132. S. Zenitani and M. Hoshino, *ApJ* **562** (2001) L63.
133. M.M. Romanova and R.V.E. Lovelace, *A&A* **262** (1992) 26.
134. G.Z. Machabeli, Q. Luo, D.B. Melrose and S. Vladimirov, *MNRAS* **312** (2000) 51.
135. Z. Osmanov and G. Machabeli, *A&A* **516** (2010) A12.
136. Z. Osmanov, *ApJ* **721** (2010) 318.
137. Iu.P. Ochelkov and V.V. Usov, *Ap&SS* **69** (1980) 439.
138. A. Levinson, *Phys. Rev. Lett.* **85** (2000) 912.
139. G.R. Blumenthal and R.J. Gould, *Rev. of Mod. Phys.* **42** (1970) 237.
140. S.R. Kelner and F.A. Aharonian, *PhRvD* **78** (2008) 4013.
141. A.M. Atoyan and C.D. Dermer, *ApJ* **586** (2003) 79.
142. M.C. Begelman, Relativistic Hadrons Near Accreting Compact Objects, in *Lecture Notes in Physics* **391** (1991) 1.
143. A. Mastichiadis, R.J. Protheroe and J.G. Kirk, *A&A* **433** (2005) 765.
144. D. Leiter and M. Kafatos, *ApJ* **226** (1978) 32.
145. M. Kafatos and D. Leiter, **ApJ** *229* (1979) 46.
146. R. Mahadevan, R. Narayan and J. Krolik, *ApJ* **486** (1997) 268.
147. R.K. Williams, *PhRvD* **51** (1995) 5387.
148. S.R. Kelner, F.A. Aharonian and V.V. Bugayov, *PhRvD* **74** (2006) 4018.
149. M. Sikora et al., *ApJ* **320** (1987) L81.
150. F.A. Aharonian and A. Atoyan, *A&A* **362** (2000) 937.
151. J.M. Jauch and F. Rohrlich *The theory of photons and electrons* (Springer, New York 1976).
152. F.A. Aharonian, *Very High Energy Cosmic Gamma Radiation* (World Scientific

    2004).
153. K. Herterich, *Nature* **250** (1974) 312.
154. F.A. Agaronyan, V.V. Vardanyan and V.G. Kirillov-Ugryumov, *Astrofizika* **20** (1984)
    223.
155. A. Levinson, *IJMPA* **21** (2006b) 6015
156. F. Aharonian and A. Neronov, *ApJ* **619** (2005a) 306.
157. F.K. Baganoff et al., *ApJ* **591** (2003) 891.
158. S. Nayakshin, *A&A* **429** (2005) L33.
159. J. Cuadra et al. *MNRAS* **366** (2006) 358.
160. F. Aharonian et al. (H.E.S.S. Collaboration), *A&A* **425** (2004) L13.
161. K. Kosack et al. *ApJ* **608** L97 (2004).
162. R.M. Crocker et al., *ApJ* **622** (2005) 892.
163. F. Aharonian et al. (H.E.S.S. Collaboration), *A&A* **503** (2009b) 817.
164. C. van Eldik, *Very High Energy γ-ray Observations of the Galactic Centre Region*,
    AIPC **1085** (2009) 146.
165. F. Acero et al. (H.E.S.S. Collaboration), *MNRAS* **402** (2010) 1877.
166. J.A. Hinton and F.A. Aharonian, *ApJ* **657** (2007) 302.
167. F. Aharonian and A. Neronov, *Ap&SS* **300** (2005b) 255.
168. S. Liu et al., *ApJ* **647** (2006) 1099.
169. D.R. Ballantyne et al., *ApJ* **657** (2007) L13.
170. A.M. Atoyan and C.D. Dermer, *ApJ* **617** (2004) L123.
171. A. Levinson and E. Boldt, *APh* **16** (2002) 265.
172. F. Melia and H. Falcke, *AR&A* **39** (2001) 309.
173. R. Genzel et al., *Nature* **425** (2003) 934.
174. K. Dodds-Eden et al., *ApJ* **698** (2009) 676.
175. A. Marconi et al., *MNRAS* **289** (1997) L21.
176. K. Gebhardt and J. Thomas, *ApJ* **700** (2009) 1690.
177. F.N. Owen, J.A. Eilek and N.E. Kassim, *ApJ* **543** (2000) 611.
178. C.S. Reynolds et al., *MNRAS* **283** (1996) L111.
179. M. Camenzind, in: *The radio galaxy Messier 87*, ed. H.-J. Röser, & K. Meisenheimer,
    LNP **530** (1999), 252.
180. T. Di Matteo et al., *ApJ* **582** (2003) 133.
181. J.A. Biretta, W.B. Sparks and F. Macchetto, *ApJ* **520** (1999) 621.
182. C. Ly, R.C. Walker and W. Junor, *ApJ* **660** (2007) 200.
183. F.M. Rieger and F.A. Aharonian, *AIPC* **1085** (2009b) 640.
184. A.A. Abdo et al. (Fermi-LAT Collaboration), *ApJ* **707** (2009) 55.
185. G.V. Bicknell and M.C. Begelman, *ApJ* **467** (1996) 597.
186. D. Whysong and R. Antonucci, *ApJ* **602** (2004) 116.
187. J-M. Wang et al., *ApJ* **676** (2008) L109.
188. L. Buson et al., *ApJ* **705** (2009) 356.
189. L. Ferrarese et al., *ApJ* **654** (2007) 186.
190. W. Israel, *A&A Rev.* **8** (1998) 237.
191. S. Tingay et al., *AJ* **115** (1998) 960.
192. M.J. Hardcastle et al., *ApJ* **593** (2003) 169.
193. A. Marconi et al., *A&A* **448** (2006) 921.
194. N. Neumayer et al., *ApJ* **671** (2007) 1329.
195. A. Marconi et al., *ApJ* **549** (2001) 915.
196. D.A. Evans et al., *ApJ* **612** (2004) 786.
197. S. Pellegrini, *ApJ* **624** (2005) 155.
198. K. Meisenheimer et al., *A&A* **471** (2007) 453.

199. M.J. Hardcastle et al., *MNRAS* **393** (2009) 1041.
200. M. Kachelrieß, S. Ostapchenko, and R. Tomás, *NJPh* **11** (2009) 065017.
201. S.O'Sullivan, B. Reville, and A.M. Taylor, *MNRAS* **400** (2009) 248.
202. F.M. Rieger and F.A. Aharonian, *A&A* **506** (2009a) L41.
203. J. Abraham et al. (Pierre AUGER Collaboration), *Science* **318** (2007) 938.
204. P. Abreu et al. (Pierre AUGER Collaboration), *APh* **34** (2010) 314.
205. J. Abraham et al. (Pierre AUGER Collaboration), *Phys. Rev. Lett.* **104** (2010) 091101.
206. M. Chiaberge, A. Capetti A. and A. Celotti, *MNRAS* **324** (2001) L33.
207. J.P. Lenain et at., *A&A* **478** (2008) 111.
208. F. Aharonian et al. (H.E.S.S. Collaboration), *ApJ* **695** (2009a) L40.
209. A.A. Abdo et al. (Fermi-LAT Collaboration), *Science* **328** (2010a) 725.
210. A.A. Abdo et al. (Fermi-LAT Collaboration), *ApJ* **719** (2010b) 1433.
211. M. Raue et al., *Proc. 44th Recontre de Moriond* (2009) arXiv:0904.2654.
212. J. Sitarek and W. Bednarek, *MNRAS* **401** (2010) 1983.
213. M. Orellana and G.E. Romero, *AIPC* **1123** (2009) 242.
214. M. Kachelrieß, S. Ostapchenko, and R. Tomás, *PASA* **27** (2010) 482.
215. M.A. Prieto et al., *MNRAS* **402** (2010) 724.
216. J.T. Radomski et al., *ApJ* **681** (2008) 141.
217. A. Levinson, *NuPhA* **827** (2009) 561.
218. K. Gebhardt et al., *ApJ* **671** (2007) 1321.
219. N.E.B. Killeen, G.V. Bicknell and R.D. Ekers, *ApJ* **325** (1988) 180.
220. K. Shurkin et al., *MNRAS* **383** (2008) 923.
221. M. Loewenstein et al., *ApJ* **555** (2001) L21.
222. R. Narayan, Why do AGN lighthouses switch off?, in *Lighthouses of the Universe: Proceedings of the MPA/ESO/MPE/USM Joint Astronomy Conference*, eds. M. Gilfanov, R. Sunyaev, and E. Churazov (Springer, 2002), p. 405.
223. G. Pedaletti, S.J. Wagner and F.M. Rieger, *ApJ* **738** (2011) 142 (arXiv:1107.0910).
224. E. Boldt and P. Ghosh, *MNRAS* **307** (1999) 491.
225. E. Boldt and M. Loewenstein, *MNRAS* **316** (2000) L29.
226. E. Khan et al., *APh* **23** (2005) 191.
227. D. Hooper, S. Sarkar and A.M. Taylor, *APh* **27** (2007) 199.